Title

Clumped 13CH2D and 12CHD2 compositions of methyl groups from wood and synthetic monomers: Methods, experimental and theoretical calibrations, and initial results

Authors

Lloyd, Max K
Eldridge, Daniel L
Stolper, Daniel A

Publication Date

2021-03-01

DOI

10.1016/j.gca.2020.10.008

Peer reviewed

Clumped $^{13}CH_2D$ and $^{12}CHD_2$ compositions of methyl groups from wood and synthetic monomers: methods, experimental and theoretical calibrations, and initial results

Max K. Lloyd[1]*, Daniel L. Eldridge[1,2], and Daniel A. Stolper[1,2]

[1]Department of Earth and Planetary Science, University of California, Berkeley, CA 94720, USA
[2]Energy Geosciences Division, Lawrence Berkeley National Laboratory, Berkeley, CA 94720, USA

* Corresponding author present address: Department of Geosciences, Pennsylvania State University, University Park, PA 16802, USA; mlloyd@psu.edu

Abstract

Methyl groups are found in numerous biogenic and synthetic materials including geologically preserved materials such as wood. The carbon and hydrogen isotope compositions of methyl groups are used as tracers in biogeochemical cycles, as paleothermometers, and to determine the hydrogen isotopic composition of ancient rain. Here we present analyses of resolved ^{13}C–D ($^{13}CH_2D$) and D–D ($^{12}CHD_2$) clumped isotope compositions of methyl groups as new variables for the study of methyl groups in the present and past. We first present chemical methods to extract, purify, and derivatize methyl groups from methoxyl (*R*–O–CH_3) groups as CH_3F and CH_3Cl, and high-resolution mass spectrometric techniques to determine the clumped isotope compositions of these species. We achieve precisions for ^{13}C–D clumping of ± 0.25 ‰ and D–D clumping of ± 2.5 ‰. We anchor our clumped isotopic measurements to a thermodynamic reference frame by first calculating the theoretical temperature dependences of ^{13}C–D and D–D clumping in CH_3Cl, then placing our measurements onto this reference frame through experimental internal isotopic equilibration of CH_3Cl at 200 °C. Finally, we provide and analyze an initial dataset of clumped ^{13}C–D and D–D compositions of methyl groups from various commercial/synthetic monomers and environmental woods. We observe ranges in clumped isotope compositions of ~11 ‰ in ^{13}C–D and ~48 ‰ in D–D, and systematic differences within these ranges between methyl groups from commercial monomers and wood. Specifically, commercial clumped ^{13}C–D compositions are between 0 and 3 ‰, which correspond to apparent equilibrium temperatures between 170 °C and the infinite temperature limit. In contrast, the clumped ^{13}C–D compositions of wood methoxyl groups are distinctively high (9.50–11.25 ‰) and 3–6 ‰ higher than would be expected if formed in internal isotopic equilibrium at Earth-surface temperatures. Commercial/synthetic methyl and wood methoxyl clumped D–D compositions are also distinct: −5 to +13 ‰ in commercial monomers vs. −35 to −8 ‰ in wood—such negative values cannot result from formation in isotopic equilibrium and require kinetic processes to have occurred. These results indicate that wood methoxyl groups are formed out of isotopic equilibrium and that clumped isotope compositions of methyl groups may be useful tracers of methyl group sources and sinks in the environment. For instance, isotopic clumping in methyl groups may be useful for understanding controls on isotopic clumping in methane produced by methylotrophic methanogens.

1. Introduction

Methyl groups are found in a range of important biological and synthetic organic compounds. Methylation reactions occur in the biosynthesis of major compound classes including lipids, sugars, nucleotides, amino acids, as well as plant structural biopolymers such as lignin and pectin (e.g., Robertson, 2005; Roje et al., 2006; Landgraf et al., 2016; Rahikainen et al., 2018). Additionally, methylated compounds such as methanol (CH_3OH), methyl tert-butyl ether, and various halomethanes (e.g., chloromethane (CH_3Cl) and fluoromethane (CH_3F)), have industrial applications (e.g., Cheng et al., 1994, Ott et al., 2012, Ohligschläger et al., 2019) or, in the case of methylated mercury compounds, are significant environmental biotoxins (Selin, 2009).

The stable isotopic composition (i.e., $^{13}C/^{12}C$ and D/H ratios) of methyl groups are used as tracers for their formational and removal pathways in environmental and industrial applications. For example, methyl carbon isotopic compositions are used to identify atmospheric sources of CH_3Cl (e.g., Keppler et al., 2008) and to distinguish natural and synthetic sources of vanillin (Krueger and Krueger, 1983; Tenailleau et al., 2004; Greule et al., 2010). The hydrogen isotopic composition of methyl groups bound to O atoms (termed methoxy or methoxyl groups) in wood lignin are used as proxies for the isotopic composition of local waters (Keppler et al., 2007; Feakins et al., 2013, Anhäuser et al., 2017) and for paleothermometery (Anhäuser et al., 2018). Here we describe the methods, calibration and initial application of measurements of methyl groups with two rare isotopes (i.e., clumped isotopes), specifically $^{13}CH_2D$ and $^{12}CHD_2$.

Clumped isotopes are of interest as their abundance relative to a random distribution of isotopes for a system at internal isotopic equilibrium is controlled solely by temperature (e.g., Eiler 2007; 2013) and is independent of the bulk isotopic composition of the molecule. As such, clumped isotopes in equilibrated systems can be used for paleothermometry. If clumped isotopic compositions are instead controlled by non-equilibrium processes such as kinetic isotope effects or mixing relationships, differences in clumped isotope compositions can be used as tracers of sources (e.g., Stolper et al., 2015; Wang et al., 2015; Douglas et al., 2016; Young et al., 2017; Giunta et al., 2019; Douglas et al., 2020), or provide constraints on formation pathways (e.g., Tripati et al., 2015; Watkins and Hunt et al., 2015; Yeung et al., 2015; Loyd et al., 2016; Magyar et al., 2016; Yeung et al., 2016; 2017; Gruen et al., 2018; Staudigel and Swart, 2018; Guo et al., 2020) or destruction mechanisms (e.g., Wang et al., 2016; Clog et al., 2018; Yeung et al., 2019; Ash et al., 2020).

Here, we (*i*) describe chemical methods to extract, purify, and convert methoxyl methyl groups to mass spectrometrically tractable analytes: CH_3F and CH_3Cl. (*ii*) We describe our mass spectrometric approaches for measuring δD and $\delta^{13}C$ and resolved $^{13}C–D$ ($^{13}CH_2D$) and D–D ($^{12}CHD_2$) clumped-isotope abundances. (*iii*) We calibrate these measurements to a thermodynamic reference frame using theory and experiments. (*iv*) Finally, we present clumped isotope analyses on an initial dataset of commercial CH_3F, CH_3Cl, CH_3I, methanol, and syringaldehyde samples as well as environmental woods and discuss first order trends. We note that the initial development and attempts to perform the measurements described here began as part of a PhD thesis (Lloyd, 2017).

2. Notation

Carbon and hydrogen isotope compositions of methyl groups are reported using δ notation where:

$$\delta^{13}\mathrm{C} = \left(\frac{^{13}R_{\mathrm{sa}}}{^{13}R_{\mathrm{VPDB}}} - 1\right) \times 1000 \quad (1)$$

and

$$\delta\mathrm{D} = \left(\frac{^{\mathrm{D}}R_{\mathrm{sa}}}{^{\mathrm{D}}R_{\mathrm{VSMOW}}} - 1\right) \times 1000, \quad (2)$$

Here, $^{13}\mathrm{R} = [^{13}\mathrm{C}]/[^{12}\mathrm{C}]$, $^{\mathrm{D}}\mathrm{R} = [\mathrm{D}]/[\mathrm{H}]$, sa is the sample, VPDB is the carbon isotopic standard and VSMOW is the hydrogen isotopic standard.

We report methyl $^{13}CH_2D$ abundance relative to that expected for a random distribution of isotopes among all isotopologues using $\Delta_{^{13}CH_2D}$ notation (see Wang et al., 2004):

$$\Delta_{^{13}CH_2D} = \left(\frac{^{13}CH_2D_{R_{\mathrm{sa}}}}{^{13}CH_2D_{R^*_{\mathrm{sa}}}} - 1\right) \times 1000. \quad (3)$$

$^{13}CH_2D_{R_{\mathrm{sa}}} = [^{13}CH_2D]/[^{12}CH_3]$ in the sample while $^{13}CH_2D_{R^*_{\mathrm{sa}}}$ is the ratio expected for a random distribution of isotopes in the sample: $^{13}CH_2D_{R^*_{\mathrm{sa}}} = 3 \times {}^{13}R_{\mathrm{sa}} \times {}^{\mathrm{D}}R_{\mathrm{sa}}$. Note that other definitions of Δ notation exist that are approximately equivalent (e.g., Wang et al., 2015).

Analogously, we report methyl $^{12}CHD_2$ abundances vs. a random distribution with $\Delta_{^{12}CHD_2}$ notation:

$$\Delta_{^{12}CHD_2} = \left(\frac{^{12}CHD_2{}_{R_{\mathrm{sa}}}}{^{12}CHD_2{}_{R^*_{\mathrm{sa}}}} - 1\right) \times 1000, \quad (4)$$

where $^{12}CHD_2{}_{R_{\mathrm{sa}}} = [^{12}CHD_2]/[^{12}CH_3]_{\mathrm{sa}}$ in the sample and $^{12}CHD_2{}_{R^*_{\mathrm{sa}}}$ is the expected ratio for a random distribution: $^{12}CHD_2{}_{R^*_{\mathrm{sa}}} = 3 \times {}^{\mathrm{D}}R_{\mathrm{sa}} \times {}^{\mathrm{D}}R_{\mathrm{sa}}$.

In the thermodynamic reference frame, Δ values of 0 ‰ equate to equilibrium at an infinite temperature and are independent of laboratory standardization (e.g., Dennis et al., 2011). However, we measure samples relative to a tank of working reference gas (wg) with *a priori* unknown $\Delta_{^{13}CH_2D}$ and $\Delta_{^{12}CHD_2}$. We initially assume that the working reference gas has $\Delta_{^{13}CH_2D}$ and $\Delta_{^{12}CHD_2}$ values of 0 ‰, and report the clumped isotope compositions of samples in a so-called 'working gas reference frame' (‰ vs. wg). Samples reported in the working gas reference frame are given as '$\Delta_{^{13}CH_2D(wg)}$' and '$\Delta_{^{12}CHD_2(wg)}$,' while the symbols '$\Delta_{^{13}CH_2D}$' and '$\Delta_{^{12}CHD_2}$', as defined in Eqns. 3 and 4, indicate the thermodynamic reference frame.

3. Methods I: methoxyl group derivatization and sample purification

Here we summarize the methods for the conversion and purification of methoxyl groups first to iodomethane (CH_3I) and then to our mass spectrometric analytes, methyl fluoride (CH_3F) or methyl chloride (CH_3Cl). We provide detailed protocols in Appendix A1, and a flowchart of the methods in Fig. A1. Portions of the methods are based on Lloyd (2017) and Greule et al. (2019) (Sections 3.1, 3.2), while others are new (Sections 3.3, 3.4).

3.1 Derivatization and purification of methoxyl groups

Methoxyl groups from starting materials such as wood or methanol are derivatized to CH_3I using the Zeisel (1885) reaction:

$$R\text{–O–}CH_3 + HI_{(aq)} \rightarrow R\text{–OH} + CH_3I \quad (5)$$

where *R* represents the rest of the molecule. We preform our derivatization reactions in a reflux apparatus (Fig. A2) following Greule et al. (2019). For each derivatization, 8 mL of HI acid are first heated to reflux (130 °C) in an He stream (25–60 mL/min) for 90 min, and cooled to room-temperature (22 °C). Next, the sample is added, the acid is reheated to reflux and maintained at reflux for 2 hr with He flowing and volatile reaction products (CH_3I, CO_2, H_2O) frozen in an adjacent trap immersed in liquid N_2 (LN_2; see Section A1.1 for details). Previous experiments demonstrated that no hydrogen isotope exchange between methyl groups and HI acid occurs during HI reflux (Keppler et al., 2007; Greule et al., 2008).

Evolved CH_3I is then purified from other gases using a series of cryogenic and chemical steps (see Fig. A3, Section A1.2 for details). Briefly, cryogenic steps are used to remove He, N_2, O_2, H_2O, and CO_2. Next, CH_3I is chemically purified using Ascarite II® and $CaCl_2$ to remove residual CO_2 and H_2O. Following purification, CH_3I yield is determined manometrically and the CH_3I is either immediately converted to CH_3F or CH_3Cl (see below), or frozen and flame-sealed into a Pyrex break-seal (for later use) and stored in the dark to prevent UV photodissociation.

3.2 Conversion of CH_3I to CH_3F or CH_3Cl

We do not use CH_3I as our mass-spectrometric analyte because it is not sufficiently volatile for stable delivery to the mass spectrometer source from a bellows. Instead, we derivatize the CH_3I to fluoromethane (CH_3F) or chloromethane (CH_3Cl), which are room-temperature gases, for mass-spectrometric analysis. Initial attempts to convert CH_3I to CH_3F were presented in a PhD thesis (Lloyd, 2017), but faced issues associated with yield and degradation of the fluorinating agent. The procedures described here mitigate these issues. The methods for the conversion of CH_3I to CH_3Cl are new. As will be discussed, CH_3Cl is our preferred mass-spectrometric analyte for future work.

3.3 CH_3F derivatization and purification

We perform fluorinations at room temperature such that C–I bonds are fluorinated but C–H bonds are not. Our full fluorination protocols are provided in Appendix A1.3 and summarized here.

The replacement of halogens (e.g., I, Br) by F in other organic molecules (e.g., 1-$C_8H_{17}I$) proceeds rapidly (<4 hr) and quantitatively at room temperature in the presence of a metal fluoride salt (e.g., AgF or CoF_3) (e.g., San Filippo and Romano, 1975; Mann 1987). Initial

attempts to react CH_3I with AgF and XeF_2 (Lloyd, 2017) produced significant (~30 %) quantities of C_2 compounds and were not pursued further. We use CoF_3 for fluorinations via the following assumed reaction:

$$2CH_3I + 2CoF_3 \rightarrow 2CH_3F + 2CoF_2 + I_2 \quad (6)$$

CoF_3 is routinely used to fluorinate H_2O for oxygen isotopic measurements (Baker et al., 2002). CoF_3 reacts rapidly (order seconds) with moisture in air to form HF. HF fluorinates C–H bonds at room temperature (e.g., Wilkinson, 1992) and, in the presence of silica (from the Pyrex holding tube), generates SiF_4 and H_2O (e.g., Helms and Deal, 1992), which then makes more HF, promoting more reactions. These reactions were problematic for us as we found it difficult to sperate SiF_4 from CH_3F. More problematic, the presence of HF results in the formation of CH_2F_2 and CHF_3, which results in low CH_3F yields and modified D/H, $^{13}C/^{12}C$, and (potentially) clumped-isotope compositions of the residual methyl groups. Lloyd (2017) handled CoF_3 in air and inevitably made some HF. To avoid this, we handle CoF_3 in an Ar atmosphere dried with Drierite. Also, we fluorinate CH_3I in reusable vessels containing subequal amounts of CoF_3 and sodium fluoride (NaF). The NaF converts any HF to $NaHF_2$ (e.g., Aigueperse et al., 2000).

Fluorinations are performed in either a reusable Pyrex (Fig. A4a) or nickel vessel (Fig. A4b). Fluorination vessels are first heated (to 150 °C for the Pyrex vessel and 60 °C for the nickel vessel) and evacuated to baseline. Next, CH_3I is frozen into the vessel using LN_2 and the vessel sealed. Fluorinations proceed at room-temperature for 8–24 hr. Products are cryogenically and chemically purified (Appendix A1.4). I_2 is removed cryogenically using LN_2 and HF is scrubbed using an NaF column. CH_3F is further purified using a variable temperature cold-head trap (Janis Research Co.) cooled using a He refrigeration unit (CTI Cryogenics model 8200): CH_3F is frozen into the trap at 80 K and cycled 3× from 140 to 80 K with residual headspace evacuated at 80 K each time. The trap is warmed to 110 K and CH_3F is distilled into an adjacent trap immersed in LN_2. Yield is determined manometrically and the gas is then frozen and flame-sealed into a Pyrex break-seal.

3.4 CH_3Cl derivatization and purification

CH_3I is converted to chloromethane (CH_3Cl) using excess silver chloride (AgCl):

$$CH_3I + AgCl \rightarrow CH_3Cl + AgI \quad (7)$$

Our approach is based on chlorine stable isotopic analyses where CH_3Cl is also the mass-spectrometric analyte. For chlorine isotopes, AgCl is quantitatively methylated using a 10× molar excess of CH_3I relative to AgCl at 80 °C for 48 hr (e.g., Eggenkamp, 2004). We instead quantitatively chlorinate CH_3I using a 10–25× molar excess of powdered AgCl (99.999% purity, Sigma Aldrich no. 204382) vs. CH_3I at 80 °C for 48 hr. To do this, we load a Pyrex break seal with 175–500 mg of AgCl and evacuate the tube while heating the powder at 250 °C for at least 15 min. CH_3I frozen into the tube using LN_2 and the headspace is evacuated. The tube is flame-sealed, wrapped in aluminum foil to prevent photodissociation, and held in a water bath at 80 °C for 48 hr.

Product gas is frozen into the cold-head trap at 120 K. Trace CO_2 is removed by warming the trap to 180 K, cooling it to 130 K, and evacuating the headspace at 130 K. The cold-head trap is warmed to 155 K and CH_3Cl transferred from the cold-head trap to a trap on a permanent vacuum line immersed in LN_2. Yield is determined monometrically. The sample is frozen into a Pyrex tube using LN_2 and flame sealed.

4. Methods II: production of study materials

We analyze four types of materials in this study: (*i*) commercial methyl-bearing compounds, likely synthetic in origin; (*ii*) environmental wood samples, contributed by S. Feakins, F. Keppler, and M. Greule, with published methoxyl $\delta^{13}C$, δD, and wt.% values; these were not processed further in order to allow direct comparison to published values (*iii*) isotopically labeled CH_3F and CH_3Cl gases, created in this study for the purposes of evaluating external measurement precision; (*iv*) sub-aliquots of gases of type (*i*) and (*iii*), heated at 200 °C in the presence of a catalyst in order to exchange C–H bonds (Section 5, below). Descriptions and sources of study materials are summarized in Table 1. One commercial CH_3F gas cylinder and one commercial CH_3Cl gas cylinder were employed as primary working reference gases for dual-inlet mass spectrometric measurements (CIT-F-1 and CIT-Cl-2, category *i*, above). External $\delta^{13}C$ and δD values of these gases were determined by A. Schimmelmann at Indiana U. using standard offline combustion/reduction + dual-inlet IRMS techniques (c.f., Schimmelmann et al., 2016; see also Section A2.1 for details). We also determined the $\delta^{13}C$ of a commercial methanol (MeOH-std) at Caltech by conventional offline combustion + dual-inlet IRMS (Section A2.1). Because the gas supply of CIT-F-1 was limited, we employed an additional reference tank for CH_3F (BIL-F-1, 99 % purity, Matheson) to serve as the actual working reference gas for the measurements described here. The secondary tank BIL-F-1 was calibrated against the primary tank CIT-F-1 by measuring them against each other 5× using the methods described in Section 6.

Isotopically labeled CH_3F and CH_3Cl gases (category *iii*, above) were made by derivatizing aliquots of isotopically labeled methanol (Cambridge Isotope Laboratories) following the methods outlined in Section 3, and diluting these labeled CH_3F and CH_3Cl gases in unlabeled commercial gases (category *i*, above; Section A2.2). Modifications of some procedures were done to avoid exposing systems that saw samples to isotopically labeled compounds (Section A2.2).

5. Methods III: equilibration of CH_3Cl on Pt/Al_2O_3 catalysts

As is generally the case when creating establishing new clumped-isotope measurements, there are no standards available with independently known $\Delta_{^{13}CH_2D}$ and $\Delta_{^{12}CHD_2}$. A common approach for clumped isotopic standardization is to equilibrate samples at known temperatures in order to place Δ values in a thermodynamic reference frame (e.g., Ghosh et al., 2006; Dennis et al., 2011; Yeung et al., 2012; Ono et al., 2014; Stolper et al., 2014a; Magyar et al., 2016; Young et al., 2016; Yeung et al., 2017; Popa et al., 2018). We follow this approach and equilibrate isotopologues of CH_3Cl on a Pt catalyst (see Fig. A1b for workflow).

For each exchange experiment, 4 pellets (~200 mg) of Pt on alumina (Pt/Al_2O_3, 0.5 wt.% loading, Sigma Aldrich no. 206016) were added to a quartz break-seal. The Pt/Al_2O_3 catalyst was pre-treated by heating at 550 °C for 4 hr in the presence of 200 mbar of O_2 (Aboul-Gheit and

Cosyns, 1976). O_2 was pumped away and the catalyst exposed to vacuum at 550 °C for an additional 4 hr. Next, 200–600 µmoles of CH_3Cl gas were frozen into the break-seal tube (using LN_2) and the tube flame sealed. The tube was placed in the center position of a box furnace (Lindberg/Blue M; ThermoFisher Scientific) and maintained at the target temperature for the duration of the experiment (up to 185 hr). At the end of each experiment, the tube was cooled to room temperature in < 20 s with compressed air.

These equilibrations produced HCl, Cl_2, and chloroethane (C_2H_5Cl) (e.g., Olah et al., 1985), which were removed using a purification procedure summarized here and detailed in Appendix A3 (Fig. A1b). Products were frozen into a Pyrex trap with LN_2 packed with KBr, sealed, and heated to ~100 °C for 10 min to scrub Cl_2 and release Br_2. Gases were passed across a dry-ice + ethanol trap to remove Br_2 and frozen onto the cold-head trap at 100 K. CH_3Cl was then purified largely following the procedure in Section 3.4, but modified to include additional purification steps (Appendix A3.1). Products were frozen and flame-sealed into a Pyrex break-seal using LN_2. To remove C_2H_5Cl, the gas mixture was heated at 500 °C for 15 or 20 min. At these conditions, C_2H_5Cl decomposes but CH_3Cl does not (e.g., Maccoll, 1969; Weisman and Benson, 1984; Wu and Won, 2000). Following pyrolysis, samples are again purified via the above chemical and cryogenic steps. This cycle of pyrolysis followed by chemical and cryogenic purifications is repeated 3× (Appendix A3.1). We demonstrate later that these steps do not affect final CH_3Cl isotopic compositions.

6. Methods IV: Mass spectrometry

Here we describe the mass spectrometric methods used to determine δD, δ^{13}C, $\Delta_{13_{CH_2D}}$, and $\Delta_{12_{CHD_2}}$ values of methyl fragment ions (CH_3^+) of CH_3F and CH_3Cl. These follow methods for methane clumped isotopic measurements (Eldridge et al., 2019), which were actually developed as part of the effort to make the methyl halogen measurements described here.

6.1 Instrument conditions

Isotopic measurements of CH_3F and CH_3Cl were made using a Thermo Scientific MAT 253 Ultra at UC Berkeley. For all measurements, sample or reference gas is expanded from either a Pyrex break-seal or a reference tank into a sample bellows. Gases are homogenized by cycling the bellows from ~40 to ~90 % expanded at least 5× over 3 min. Samples are measured against working reference gases of known δD and δ^{13}C (BIL-F-1 for CH_3F measurements or CIT-Cl-2 for CH_3Cl measurements).

For the both CH_3F and CH_3Cl, the target source pressure is 2.7×10^{-7} mbar, equivalent to ~80 mbar for CH_3F and ~60 mbar for CH_3Cl at 100% bellows expansion. We tune source conditions to maximize CH_3^+ intensity and minimize H-adduct production (e.g., $^{12}CH_4^+$), which occurs at low trap voltage (1–3 V) and low extraction (10–20 %). For CH_3F, $^{12}CH_3^+$ intensity is 3× larger than $^{12}CH_3F^+$ and $^{12}CH_2D^+$ is 1.7× larger than $^{12}CH_4^+$ (Fig. 1). For CH_3Cl, CH_3^+ intensity is 2× larger than $^{12}CH_3{}^{35}Cl^+$, and $^{12}CH_2D^+$ is ~0.5× that of $^{12}CH_4^+$ (Fig. 2). At the same source pressures, CH_3Cl yields 3× higher $^{12}CH_3^+$ intensity vs. CH_3F (Table A1).

6.2 Gas purity evaluation

Prior to each measurement, we scan and compare the mass spectrum of the sample and reference gases to evaluate sample purity (see Table A1, Figs. A6, A7 for details). For CH_3F, common

potential contaminants are CH_2F_2, CO_2, and SiF_4. CH_3F samples are not measured if the CH_2F_2 content exceeds 0.2% (taken as $100 \times \left(i_{\mathrm{CHF_2^+_{sa}}} - i_{\mathrm{CHF_2^+_{wg}}}\right)/\left(i_{\mathrm{CH_3^+_{sa}}} + i_{\mathrm{CH_3F^+_{sa}}}\right)$, where i is intensity of the measured beam). This is because pilot measurements indicated that δD accuracy is compromised above this threshold (Fig. A9). We have yet to observe a sample with an excess of CO_2 or SiF_4 that was not also rejected for other reasons (low yield or high CH_2F_2 abundance), but we continue to monitor these peaks.

For CH_3Cl, the main potential contaminant is chloroethane (C_2H_5Cl; see Table A1 for all monitored contaminants). Samples are not analyzed if C_2H_5Cl content exceeds 0.25 % (defined as $100 \times \left(i_{\mathrm{C_2H_5^+_{sa}}} - i_{\mathrm{C_2H_5^+_{wg}}}\right)/\left(i_{\mathrm{CH_3^+_{sa}}} + i_{\mathrm{CH_3Cl^+_{sa}}}\right)$). Pilot measurements indicated that δD and δ^{13}C accuracies were compromised above this threshold. We note that wood samples typically yield C_2H_5Cl contents of 0.03 % and never higher than 0.1 %.

6.3 $\delta^{12}CH_2D$ measurement

D/H ratios of methyl fragments are determined from $\delta^{12}CH_2D$ values where:

$$\delta^{12}\mathrm{CH_2D} = \left(\frac{{}^{12}\mathrm{CH_2D}R_{\mathrm{sa}}}{{}^{12}\mathrm{CH_2D}R_{\mathrm{wg}}} - 1\right) \times 1000\,. \quad (8)$$

Here, ${}^{12}\mathrm{CH_2D}R = [{}^{12}CH_2D^+]/[{}^{12}CH_3^+ + {}^{12}CHD^+]$. $\delta^{12}CH_2D$ is defined such that the working reference gas (wg) has a $\delta^{12}CH_2D$ value of 0 ‰. The denominator of this ratio includes a contribution from the twice-fragmented ion ${}^{12}CHD^+$—likely generated by multiple fragmentation reactions in the source. This is corrected for during data processing (Appendix A4) and changes δD values by < 0.01 ‰. Detector settings, instrument configuration, and typical peak intensities are given in Table A2. Briefly, ${}^{12}CH_2D^+$ is measured in Faraday cup H4 (40 µm exit slit, 10^{13} amplifier) and the flat shoulder of ${}^{12}CH_3^+ + {}^{12}CHD^+$ in Faraday cup L2 (10^{10} amplifier) (Figs. 1, 2). The standard aperture, medium resolution slit is used for CH_3F (mass resolving power of 22,000 M/ΔM, 5–95 % definition) and the high resolution slit for CH_3Cl (mass resolving power of 28,000).

$\delta^{12}CH_2D$ are determined in measurement blocks that each consist of 10 sample/standard cycles (i.e., 21 integrations/block). 5 blocks are measured for CH_3F and 4 for CH_3Cl. At the start each block, sample and standard gases are automatically pressure balanced to intensities of 1.4×10^9 cps ± 0.8 % on ${}^{12}CH_3^+ + {}^{12}CHD^+$ (equiv. to 2240 mV). Typical ${}^{12}CHD^+$ intensities are 280,000 cps/450 mV for CH_3F, 320,000 cps/510 mV for CH_3Cl; higher mass 16 intensities at the same mass 15 intensity are seen for CH_3Cl vs. for CH_3F because a smaller proportion of the mass 16 beam is excluded by the exit slit on the H4 cup in high resolution mode vs. in medium resolution mode. Each integration begins with an automatic peak center on ${}^{12}CH_2D^+$ followed by 90 consecutive 0.524 s sub-integrations (47.16 s total integration time). At the end of all measurement blocks, measurement backgrounds are determined with gas still flowing into the source by jumping the magnet +0.1 Da and performing five 47.16 s integrations while cycling between the sample and standard gases. Sample and standard backgrounds are always indistinguishable (within 3 standard errors, hereafter s.e.). As such, we average them and subtract

the average from the sample and standard mass 15 and 16 measurements. Completion of a $\delta^{12}CH_2D$ measurement for both analytes takes 3–4 hours and yields typical internal measurement precisions, given as ±1 s.e., of 0.14 ‰ for CH_3F and 0.12 ‰ for CH_3Cl. Here and throughout this paper, internal measurement precision is defined as the standard deviation of all sample/standard comparisons divided by the square root of the number of comparisons.

6.4 Simultaneous $\delta^{13}CH_3$ and $\delta^{13}CH_2D$ measurement

Sample $^{13}C/^{12}C$ and $^{13}CH_2D/^{12}CH_3$ ratios are determined from $\delta^{13}CH_3$ and $\delta^{13}CH_2D$ where:

$$\delta^{13}\mathrm{CH_3} = \left(\frac{^{13\mathrm{CH_3}}R_{\mathrm{sa}}}{^{13\mathrm{CH_3}}R_{\mathrm{wg}}} - 1 \right) \times 1000 \quad (9)$$

and

$$\delta^{13}\mathrm{CH_2D} = \left(\frac{^{13\mathrm{CH_2D}}R_{\mathrm{m,sa}}}{^{13\mathrm{CH_2D}}R_{\mathrm{m,wg}}} - 1 \right) \times 1000. \quad (10)$$

Here, $^{13\mathrm{CH_3}}R = [^{13}CH_3^+]/[^{12}CH_3^+ + {}^{12}CHD^+]$ and $^{13\mathrm{CH_2D}}R_{\mathrm{m}} = [^{13}CH_2D^+]/[^{12}CH_3^+ + {}^{12}CHD^+]$. We define the $\delta^{13}CH_3$ and $\delta^{13}CH_2D$ values of the working reference gas to be 0 ‰. Note the inclusion of the subscript 'm,' which stands for 'measured,' to distinguish this ratio from $^{13\mathrm{CH_2D}}R = [^{13}CH_2D]/[^{12}CH_3]$ (Eqn. 3), which does not include the $^{12}CHD^+$ fragment. The contribution of the $^{12}CHD^+$ fragment is corrected for during data processing (Appendix A4) and changes $\delta^{13}CH_3$ and $\delta^{13}CH_2D$ values by < 0.01 ‰.

The detector array is configured such that the high-mass shoulder of $^{12}CH_3^+ + {}^{12}CHD^+$ is in Faraday cup L4 (10^{10} amplifier), the low-mass shoulder of $^{13}CH_3^+$ in Faraday cup L1 (10^{12} amplifier for CH_3F and 10^{11} amplifier for CH_3Cl), and $^{13}CH_2D^+$ on the H4 compact discrete dynode (CDD) detector (Figs. 1, 2, Table A2). Cups are not moved to make this measurement following the $\delta^{12}CH_2D$ determination. We use the medium resolution slit and standard aperture at a mass resolving power > 22,000 on H4 for both CH_3F and CH_3Cl (Figs. 1 and 2).

$\delta^{13}CH_3$ and $\delta^{13}CH_2D$ values are determined in measurement blocks comprised of an automated pressure balancing routine followed by 10 sample/standard integration cycles (total 21 integrations per block). Pressures are automatically balanced such that the $^{12}CH_3^+ + {}^{12}CHD^+$ intensity is set to 1.4×10^9 cps (2240 mV) for CH_3F or 4.2×10^9 cps (6730 mV) for CH_3Cl (±0.7%). Corresponding $^{13}CH_3^+$and $^{13}CH_2D^+$ intensities are 1.5×10^7 cps (2400 mV) and 2800 cps for CH_3F, 4.4×10^7 cps (700 mV) and 8800 cps for CH_3Cl. Due to the ~2/3 lower intensity of CH_3^+ for CH_3F vs. CH_3Cl at the same source pressure, more measurement blocks are performed for CH_3F (18–24 blocks, depending on the amount of sample gas remaining and daily scheduling considerations) vs. CH_3Cl (7–12 blocks) in order to reach comparable precision.

Each integration begins with an automatic peak center on $^{13}CH_2D^+$ followed by 60 consecutive 1.048 s sub-integrations of $^{12}CH_3^+ + {}^{12}CHD^+$, $^{13}CH_3^+$, and $^{13}CH_2D^+$ (62.88 s total integration time). At the end of all measurement blocks, two background measurements are performed with gas still flowing into the source. First, the background for the $\delta^{13}CH_3$ determination is measured

0.007 Da below the $^{13}CH_2D^+$ center for 3 sample/standard cycles, with each integration consisting of 60 sub-integrations of 1.048 s each (Fig. 2). This background is used to correct for the possible presence of $^{14}NH_2^+$ on $^{13}CH_3^+$. This is done as we observed that, in some CH_3F measurements that were ultimately rejected for other reasons (low yield, high CH_2F_2 abundance), the $^{14}NH_2^+$ background was resolvably higher in the sample gas vs. the standard. In all data reported here, sample and standard $^{14}NH_2^+$ backgrounds are always statistically identical (within 3 s.e.), and so are averaged and subtracted from both the sample and standard $^{13}CH_3^+$ measurements.

Second, with gas still flowing into the source, backgrounds for the $^{12}CH_3^+ + {}^{12}CHD^+$ and $^{13}CH_2D^+$ measurements are performed +0.1 Da above the $^{13}CH_2D^+$ center with 3 sample/standard cycles consisting of 60 consecutive 1.048 s sub-integrations. Sample and standard backgrounds are always identical (within 3 s.e.). As such, we average them and subtract the average from the sample and standard mass 15 and 17 measurements. The $\delta^{13}CH_2D$ measurement does not require a tailing correction because $^{13}CH_2D^+$ is resolved from $^{13}CH_4^+$ in our measurements—tailing from $^{13}CH_4^+$ contributes <0.7 cps to the center of the $^{13}CH_2D^+$ peak when measured as CH_3Cl (and a proportionally smaller amount as CH_3F). Under typical measurement conditions, this alters $\delta^{13}CH_2D$ values by <0.1 ‰, i.e., 2.5× smaller than the measurement precision, which we consider negligible (especially since this $^{13}CH_4^+$ tailing will be of similar size in both gases).

This measurement takes 5 to 7 hours for CH_3Cl and 12 to 16 hours for CH_3F, depending on the number of measurement blocks performed. Internal measurement precisions (± 1 s.e.) are ~0.003 ‰ for $\delta^{13}CH_3$ and 0.23–0.30 ‰ for $\delta^{13}CH_2D$.

6.5 $\delta^{12}CHD_2$ measurement

For CH_3Cl samples only, $\delta^{12}CHD_2$ values are determined where:

$$\delta^{12}\mathrm{CHD}_2 = \left(\frac{{}^{12\mathrm{CHD}_2}R_{\mathrm{m,sa}}}{{}^{12\mathrm{CHD}_2}R_{\mathrm{m,wg}}} - 1 \right) \times 1000. \quad (11)$$

Here, ${}^{12\mathrm{CHD}_2}R_{\mathrm{m}} = [{}^{12}CHD_2^+]/[{}^{12}CH_3^+ + {}^{12}CHD^+]$ and the $\delta^{12}CHD_2$ of the working reference gas (wg) is defined to be 0 ‰. As above, the 'm' subscript distinguishes this ratio from ${}^{12\mathrm{CHD}_2}R$ (Eqn. 4), which does not contain the $^{12}CHD^+$ fragment in the denominator.

The detector array is configured so that the high-mass shoulder of $^{12}CH_3^+ + {}^{12}CHD^+$ is measured on Faraday cup L4 (10^{10} amplifier) and the center of $^{12}CHD_2^+$ on the H4 CDD (Table A2; Fig. 2; note that this requires moving the L4 cup from its previous alignment). The instrument is set to high resolution, standard aperture, and tuned to a mass resolving power of > 28,000 on H4 (Fig. 2).

Bellows pressures are manually adjusted to yield an intensity of 1.3×10^9 cps on cup L4 (2080 mV) and mass spectrum scans of the methyl fragment isotopologues at cardinal mass 17 are acquired on the H4 CDD for both the sample and working reference gases (Fig. 2). We then perform a slow, precise mass spectrum scan (0.04 mDa step size, 4.194 s integration per step) of

the $^{16}OH^+$ peak in the reference gas . These scans are used for a peak-tailing correction on the $^{12}CHD_2^+$ peak (described below and in Fig. A8).

The $\delta^{12}CHD_2$ measurement routine consists 10–18 measurement blocks with 10 sample/standard cycles. The number of blocks used depends on the amount of sample gas remaining following the previous analyses. Measurement blocks begin with an automated pressure balancing of sample and standard gases to within 0.8 % of 1.3×10^9 cps on cup L4. Typical $^{12}CHD_2^+$ intensities are 20–40 cps. Each integration begins with an automated peak center on $^{13}CH_4^+$ on the H4 CDD. Next, the measurement mass is increased by +0.00137 Da , which is the calculated center of the $^{12}CHD_2^+$ peak. Peaks are integrated for 60 consecutive sub-integrations of 1.048 s each. After all measurement blocks are completed, a background is determined with gas flowing into the source by increasing the instrument mass +0.1 Da and integrating for 2 sample/standard cycles of 62.88 s each. For mass 15, sample and standard backgrounds are averaged (as they are always within 3 s.e.) and subtracted from both the sample and standard $^{12}CH_3^+$ + $^{12}CHD^+$ measurements.

For the $^{12}CHD_2^+$ integrations, we correct for both a scattered ion background (as determined by measuring the background +0.1 Da above the $^{12}CHD_2^+$ peak; typically ~0.1 cps and always indistinguishable in the sample and standard) and for tailing from the adjacent $^{13}CH_4^+$ and $^{12}CH_3D^+$ peaks. The tailing of these species contributes ~0.3–0.5 cps to ~20–40 cps of total $^{12}CHD_2^+$ signal. Our procedure for determining these corrections is based on the methodology for $^{12}CH_2D_2^+$ measurements of methane first presented by Xie et al. (2019) and described at UC Berkeley for methane in Eldridge et al. (2019). We employ an equivalent approach for corrections of $\delta^{12}CHD_2$ as shown in Fig. A8.

The complete $\delta^{12}CHD_2$ measurement routine takes 7–12 hours with achieved measurement precisions of $\delta^{12}CHD_2$ ranging from 1.5–3.0 ‰ (1 s.e.), depending on the number of measurement blocks and the $\delta^{12}CHD_2$ value of the sample.

6.6 Calculation of δD, δ^{13}C, $\Delta_{13_{CH_2D}}$, and $\Delta_{12_{CHD_2}}$ values

Raw intensities in instrument output files from the Qtegra software (v.2.9) are converted to $\delta^{12}CH_2D$, $\delta^{13}CH_3$, $\delta^{13}CH_2D$, and $\delta^{12}CHD_2$ values (relative to the working reference gas) using custom data processing scripts available with the online version of this article. During automated data processing, background corrections are first applied as described in the preceding sections. Next, sub-integrations performed on the H4 Faraday cup or H4 CDD i.e., $^{12}CH_2D^+$, $^{13}CH_2D^+$, and $^{12}CHD_2^+$, are screened for outliers due to peak position drift. Measurements on the H4 Faraday cup and H4 CDD are sensitive to peak position drift because, due to the narrow exit slits on these cups, peak widths approach the cup sizes and thus peak tops are not flat. Two data filtering algorithms are used here for this purpose (see Appendix A5)—these are derived and discussed in detail for methane in Eldridge et al. (2019); see Section SI.3 of that study. The effect of the filters is small: 12 % and 3 % of sub-integrations for CH_3F and CH_3Cl $\delta^{12}CH_2D$ measurements, respectively, are excluded and this changes mean δD values by typically < 0.05 ‰. The filters improve δD precisions by 0.01–0.1 ‰. For $^{13}CH_2D^+$ and $^{12}CHD_2^+$ measurements, less than 2 % of sub-integrations are excluded by the filters, which change $\delta^{13}CH_3D$ and $\delta^{12}CHD_2$ values by typically < 0.1‰. Precisions on $\delta^{13}CH_3D$ and $\delta^{12}CHD_2$ measurements are substantially improved

by these filters only in instances where a peak drifted a large amount (> 100 μDa) during an integration.

Background corrected and filtered $\delta^{12}CH_2D$, $\delta^{13}CH_3$, $\delta^{13}CH_2D$, and $\delta^{12}CHD_2$ values are converted to δD, δ^{13}C, $\Delta_{^{13}CH_2D(wg)}$, and $\Delta_{^{12}CHD_2(wg)}$ values based on equations provided (and derived) in the Appendix (Sections A4.1–A4.3). These calculations yield δD values relative to VSMOW, δ^{13}C values relative to VPDB, and $\Delta_{^{13}CH_2D(wg)}$ and $\Delta_{^{12}CHD_2(wg)}$ values relative to the working reference gas. $\Delta_{^{13}CH_2D(wg)}$ and $\Delta_{^{12}CHD_2(wg)}$values are then converted to the thermodynamic reference frame ($\Delta_{^{13}CH_2D}$ and $\Delta_{^{12}CHD_2}$) based on the results of the equilibration experiments reported below. These calculations correct for the inclusion of $^{12}CHD^+$ in measured isotope ratios.

Finally, a Monte Carlo approach (10^6 iterations) is used to calculate the uncertainty on δD, δ^{13}C, $\Delta_{^{13}CH_2D(wg)}$, and $\Delta_{^{12}CHD_2(wg)}$. It propagates errors from all relevant δ measurements into final reported precisions.

7. Methods V: Theoretical calculations of equilibrium Δ as a function of temperature

Establishing a thermodynamic reference frame for $\Delta_{^{13}CH_2D}$, and $\Delta_{^{12}CHD_2}$ values requires constraints on their equilibrium temperature dependencies. The equilibrium isotope exchange reactions for methyl clumped isotopes can be written as follows:

$$R - {}^{13}CH_3 + R - {}^{12}CH_2D \rightleftharpoons R - {}^{12}CH_3 + R - {}^{13}CH_2D \quad (12)$$

$$2\left(R - {}^{12}CH_2D\right) \rightleftharpoons R - {}^{12}CH_3 + R - {}^{12}CHD_2 \quad (13)$$

Here, we calculate the equilibrium constants for these reactions (which can be related to Δ values as described below) as a function of temperature using the approaches of Urey (1947) and Bigeleisen and Mayer (1947). Specifically, we calculate of so-called reduced partition functions (RPFRs; e.g., Bigeleisen-Mayer, 1947; Schauble, 2004) of isotopically substituted isotopologues relative to the unsubstituted isotopologue via the following equation:

$$\mathrm{RPFR} = e^{-(E_0^* - E_0)/k_B T} \prod_{i=1}^{a} \frac{\omega_i^*}{\omega_i} \frac{1 - e^{-hc\omega_i/k_B T}}{1 - e^{-hc\omega_i^*/k_B T}}. \quad (14)$$

In Eqn. 14, E_0 is the harmonic zero-point energy, ω_i is the harmonic frequency (given as wave number) of the i^{th} normal mode, a is the total number of vibrational modes ($a = 3N - 5$ for linear molecules, $a = 3N - 6$ for non-linear molecules), and * indicates the isotopically substituted molecule. In this formulation, mass terms and symmetry numbers are normalized out of the partition function ratios. This approach assumes the Born-Oppenheimer approximation, assumes rotations are rigid, treats rotational and translational motions as classical, and assumes quantized vibrational energies can be approximated as harmonic oscillators. We calculate RPFRs for isotopically substituted methyl groups (e.g., R–$^{13}CH_3$, R–$^{12}CH_2D$, R–$^{13}CH_2D$, R–$^{12}CHD_2$) vs. the unsubstituted group (R–$^{12}CH_3$). RPFRs are given as $^{R-i}$RPFR where i indicates the isotopically substituted methyl group.

Calculated RPFRs can be related to Δ values and equilibrium constants with the following equations:

$$\Delta_{R-^{13}CH_2D} \cong 1000 \times \ln\left(K_{R-^{13}CH_2D}\right) = 1000 \times \ln\left(\frac{{}^{R-^{13}CH_2D}_{RPFR}}{{}^{R-^{12}CH_2D}_{RPFR} \times {}^{R-^{13}CH_3}_{RPFR}}\right) \quad (15)$$

$$\Delta_{R-^{12}CHD_2} \cong 1000 \times \ln\left(3K_{R-^{12}CHD_2}\right) = 1000 \times \ln\left(\frac{{}^{R-^{12}CHD_2}_{RPFR}}{\left({}^{R-^{12}CH_2D}_{RPFR}\right)^2}\right). \quad (16)$$

In Eqs. 15 and 16, $K_{R-^{13}CH_2D}$ and $K_{R-^{12}CHD_2}$ are the equilibrium constants for Eqs. 12 and 13 respectively. The factor of 3 in Eqn. 16 arises from the symmetry numbers for the included isotopologues. The equations are approximate because we assume that the abundances of singly substituted methyl groups (R–$^{13}CH_3$ and R–$^{12}CH_2D$) are randomly distributed. This is not strictly true, but is a valid assumption at the level of precisions we attain (~0.25 ‰ for $\Delta_{^{13}CH_2D}$, ~2.5 ‰ for $\Delta_{^{12}CHD_2}$) and for the range of δD and δ^{13}C values studied here. RPFRs are calculated for gaseous chloromethane (CH_3Cl), fluoromethane (CH_3F), and methanol (CH_3OH). These correspond to our analytes and what we consider to be the simplest methoxyl group (methanol). We additionally provide calculations for Δ values in methane using the same approach for comparison to methyl groups and previous work.

The harmonic frequencies used in the RPFRs are derived from potential energy surfaces calculated using the *Gaussian09* software package (Frisch et al., 2013). CH_3Cl, CH_3F, MeOH, and CH_4 calculations were performed at the B3LYP level of theory (Becke, 1993; Lee et al., 1988) with the 6-31G+(d,p) basis set, and at the CCSD (Purvis and Bartlett, 1982) and MP2 (Møller and Plesset, 1934) levels of theory using the aug-cc-pVTZ basis set (Dunning, 1989; Kendall et al., 1992).

8. Results

Individual clumped isotopic values for all measurements are provided in spreadsheets in the Electronic Annex. Mean values for replicate measurements are listed in Table 2. Below we summarize key results.

8.1 Replicate analyses of internal gas standards

We created four gas standards (plusD-F-std, plusD-Cl-std, plus^{13}C-Cl, and BI-Cl-1) with different δD, δ^{13}C, $\Delta_{^{13}CH_2D(wg)}$ and $\Delta_{^{12}CHD_2(wg)}$ from our working gases (see Section 3.5) to be able to establish our long term mass-spectrometric precision. The CH_3Cl standards vary in δD, δ^{13}C, and $\Delta_{^{13}CH_2D(wg)}$ relative to our working gas by +65 to +147 ‰, −0.3 to +40 ‰, and −6 to +26 ‰, respectively (Table 2). The CH_3F standard differs from the working gas by +118 ‰, +0.3 ‰, and +4 ‰, respectively. Two of the CH_3Cl standards have $\Delta_{^{12}CHD_2(wg)}$ values of ~+6 and +87 ‰. The plusD-Cl-std is sufficiently enriched in $^{12}CHD_2$ that, rather than attempt to measure it directly in the manner described in Section 6.5, we estimated its $\Delta_{^{12}CHD_2(wg)}$ value from the height of $^{12}CHD_2^+$ in mass scans of this gas vs. the standard. Based on this, we estimate

a $\delta^{12}CHD_2$ of ~17,920 ‰ (vs. CIT-Cl-2), which corresponds to a $\Delta_{12_{CHD_2(wg)}}$ value of ~13,390 ‰ (Table 2).

Replicate analyses of gas standards allow comparison between internal ±1 s.e. and external ±1σ reproducibility for determining the long-term measurement precision (Table 3; see also Huntington et al., 2009). By internal precision we mean the standard error of all individual sample vs. reference gas comparisons within a single measurement. External precision is the standard deviation of multiple measurements and compares procedural replicates, including any chemistry and gas handling involved. Internal ±1 s.e. and external ±1σ should therefore agree 1:1 if the measurement is stable and sample handling procedures are non-fractionating (Huntington et al., 2009).

Mean internal ±1 s.e. for δD, $\delta^{13}C$, and $\Delta_{13_{CH_2D(wg)}}$ on CH_3F are 0.14, 0.01, and 0.29 ‰ while the external ±1σ values of the gas standard are 0.11, 0.03, and 0.21 ‰ (n = 6; Table 2). For CH_3Cl, ±1 s.e. measurement precisions are 0.12, 0.01, and 0.22 ‰ and external ±1σ precisions of all gas standards are 0.17, 0.02, and 0.22 ‰ (n = 15; Table 3). These values aggregate the replicate measurements of all three CH_3Cl gas standards. BI-Cl-1 was analyzed 4 times for $\Delta_{12_{CHD_2(wg)}}$, yielding internal 1 s.e. and external 1σ errors of 2.28 and 2.42 ‰ (Table 3). Thus, in all cases, external ±1σ precisions are effectively the same as internal ±1 s.e. for gas standards.

8.2 Measurements of CH_3I standard

We report isotopic data from 4 replicate fluorinations and 13 replicate chlorinations of the CH_3I standard; individual measurements are given in the Electronic Annex Tables EA2 and EA3, and mean values in Table 2.

Fluorinations reactions were carried out in both the Pyrex and nickel vessels (Section 3.2). For the fluorinations, we observed a dependence of $\delta^{13}C$ and δD values on yield and CH_2F_2 content (Fig. A9; Table EA2). Based on these dependencies, we exclude data from fluorinations with < 95 % yield and > 0.2 % CH_2F_2. This results in the exclusion of 9 of the 13 CH_3I standard fluorination attempts. Yield and purity were independent of reaction time (4–24 hr). Mean values and ±1σ (i.e., the external precision) of the four remaining replicates (three Pyrex and one nickel fluorination) are: δD = –98.13 ± 1.58 ‰ (vs. VSMOW), $\delta^{13}C$ = –52.74 ± 0.56 ‰ (vs. VPDB), and $\Delta_{13_{CH_2D(wg)}}$ = –2.71 ± 0.09 ‰ (vs. wg) (Table 2).

For chlorinations of the CH_3I standard, yields are 97.4 to 101.3 %, and always within error of 100 % given the uncertainties of our manometry (± 1.5–3 % depending on sample size). Chlorination yields are independent of reaction time (between 22 and 70 hours) and AgCl excess (5–31× molar excess vs. CH_3I) (Table EA3). Mean and ±1σ values (external precisions) for the 13 replicate chlorinations are: δD = –101.39 ± 1.99 ‰, $\delta^{13}C$ = –52.79 ± 0.21 ‰, and $\Delta_{13_{CH_2D(wg)}}$ = –2.20 ± 0.27 ‰ (vs. wg) (Table 2). The four analyses that included $\Delta_{12_{CHD_2(wg)}}$ determinations yield a mean value of −10.12 ± 2.57 ‰ (±1σ). δD and $\delta^{13}C$ values of the CH_3I std thus agree within 1σ when measured as CH_3F vs. CH_3Cl. The offset in $\Delta_{13_{CH_2D(wg)}}$ values is further described in Section 8.6.

Compared to the gas standards, these external 1σ reproducibilities of the CH_3I liquid standard are order 10× worse for δD and δ^{13}C, but the external 1σ precision for $\Delta_{13_{CH_2D(wg)}}$ values from replicate derivatizations of the CH_3I standard to CH_3F and CH_3Cl are indistinguishable from internal 1 s.e. measurement precision: 0.29‰ internal vs. 0.09 ‰ external for CH_3F and 0.24 internal vs. 0.27 ‰ external for CH_3Cl (Table 2). Four replicate $\Delta_{12_{CHD_2(wg)}}$ analyses of the CH_3I standard derivatized to CH_3Cl also match internal measured precision: 2.62 vs. 2.57 ‰ (internal 1 s.e. vs. external 1σ).

8.3 Methanol, wood, and syringaldehyde samples

We analyzed one methanol, one syringaldehyde, and five wood samples as either CH_3F, CH_3Cl, or both. Isotopic compositions for individual measurements are given in in Electronic Annex Table EA4 and mean values, separated by analyte gas, in Table 2.

The methanol standard was analyzed five times as CH_3Cl and yielded ±1σ external reproducibilities for δD, δ^{13}C , and $\Delta_{13_{CH_2D(wg)}}$ of 0.94, 0.99, 0.39 ‰ (Table 3). The methanol standard was only measured once as CH_3F and thus cannot be used to asses external reproducibility. Replication of wood samples yielded external ±1σ reproducibilities as CH_3F (n = 3) of 1.20, 2.12, and 0.32 ‰ and as CH_3Cl (n = 4) of 0.46, 0.74, and 0.24 ‰ (Table 3). Thus, as was the case with measurements of CH_3I (which is a part of this procedure), conversion of methoxyl groups from wood or methanol to CH_3Cl or CH_3F decreases external precision of δD and δ^{13}C values by ~0.5 to 1 ‰ relative to internal precision, while $\Delta_{13_{CH_2D(wg)}}$ yields external reproducibilities equivalent to those for internal measurement precision (0.25‰).

8.4 Methoxyl yields

In our reactions, it is important that we quantitatively extract and recover methoxyl groups as CH_3F or CH_3Cl to avoid isotopic fractionations due to poor yield. To evaluate this, we measured samples of wood and syringaldehyde with published methoxyl contents (Greule et al., 2019; Lee et al., 2019). Our yields are determined by manometry (Section 3.4) while the published values for woods were measured via gas chromatography (Li et al., 2012; Lee et al., 2019). The syringaldehyde material has a methoxyl content known based on stoichiometry.

For the syringaldehyde standard, our determined methoxyl content was 34.03 wt.% vs. a value of 34.1 wt.% theoretical. For the wood samples, our measured values largely agree with previously measured values (Fig. 4). However, there is scatter of up to 1 wt.% and, other than one wood sample with close agreement (HUBG4: wt.% 5.12 vs 5.09, this study vs. Greule et al., 2019), our methoxyl concentrations are higher than external values by 0.2–1.0 wt.% (Fig. 4).

8.5 Accuracy of methoxyl δD and δ^{13}C measurements

We examine the accuracy of our δD and δ^{13}C measurements in two ways. First, we compare δD and δ^{13}C values of five materials analyzed as both CH_3F and CH_3Cl (Table 2). δD values of CH_3F vs. CH_3Cl analyses of the CH_3I std, the MeOH std, and three woods are in 1:1 agreement over a range of 200 ‰ (mean difference = 0.65 ± 1.80 ‰; 1 s.e.; Fig. 5a). δ^{13}C values of the same materials are also in 1:1 agreement over a range of 30 ‰ (mean difference =1.24 ± 0.72 ‰ 1 s.e.; Fig. 6a).

Second, we compare δD and δ^{13}C measurements of six wood or syringaldehyde standards presented here vs. published values (Lee et al., 2019; Greule et al. 2019) or, for the methanol, measured for δ^{13}C at Caltech via conventional methods (Section 4). Published δ^{13}C values range from −26.8 to −40.9 ‰ (Table 1). Measured values made here are offset from external measurements by up to 2.15 ‰ in either direction and the slope is indistinguishable from 1 (Fig. 6b). As our external 1σ precision for wood methoxyl δ^{13}C values is ± 1.6 ‰, these deviations are within ±2 s.e.

Published δD values range from −315 to −171‰ (Table 1). Our methoxyl δD values correlate 1:1 with external published values (Fig. 5b). All samples agree within 25 ‰ with an average disagreement of 12 ± 8 ‰ (1σ). Our measurements agree within ±2 s.e. of those reported in Lee et al. (2019) (USC laboratory) but show systematically lower values (by 18 ± 6 ‰; 1σ) from those reported in Greule et al. (2019) (HU laboratory). Normalizing measured δD values relative to the highest values measured in each laboratory (Fig. 5c), values measured here vs. in other labs agree (except for one outlier) within ± 10 ‰ of a 1:1 line. Relative differences in measured δD values of the various laboratories are thus comparable, but there are potential interlaboratory offsets in δD scaling relative to VSMOW of ~20‰, which are discussed below.

8.6 Comparison and cross-calibration of $\Delta_{13_{CH_2D}}$ measurements made as CH_3Cl and CH_3F

We compare differences in $\Delta_{13_{CH_2D(wg)}}$ values when samples were analyzed as both CH_3Cl and CH_3F in Fig. 7 and Table 2. $\Delta_{13_{CH_2D(wg)}}$ values range by 11‰ for both analytes. A York regression of these data (i.e., a least squares regression with error on both x and y; York, 1968) yields a slope of 0.981 ± 0.023 and intercept of 0.458 ± 0.118 (both ±1 s.e.; Fig. 7). A linear regression without error yields essentially the same slope and intercept: 0.982 ± 0.020 and 0.466 ± 0.126 (both ±1 s.e.), respectively.

Although the slope observed between measured $\Delta_{13_{CH_2D(wg)}}$ values on CH_3Cl vs. CH_3F is within error of 1, there exists a statistically significant offset between the two as evidenced by the non-zero y-intercept of 0.458 ± 0.118 (1 s.e.). Thus, the 'true' $\Delta_{13_{CH_2D}}$ values of the CH_3F (BIL-F-1) and CH_3Cl (CIT-Cl-2) working reference gases differ by ~0.5‰. Based on this, we correct $\Delta_{13_{CH_2D(wg)}}$ values measured as CH_3F to CH_3Cl or (vice versa) with a constant correction term. We determine this correction as follows: (*i*) as the slope is within ±1 s.e. error of a 1:1 line, we assume relative measured differences of samples as CH_3F or CH_3Cl are indeed 1:1. (*ii*) We find the constant correction term based on the error-weighted mean of measured differences between all samples, which yields a value of 0.479 ± 0.096 ‰ (1 s.e.), which is within ±1 s.e. of the y-intercept from the York regression and within ±1 s.e. of the unweighted mean of 0.396 ‰. This term can then be used to translate values measured relative to the CH_3F working gas to those measured relative to the CH_3Cl working gas or vice versa (see A1.5 for exact equation).

8.7 CH_3Cl exchange experiments

We report five experiments in which CH_3Cl gases were heated in the presence of the Pt/Alumina catalyst (Table 4). The experiments were performed at a fixed temperature of 200 °C for 90 to 185 hr. In all experiments, >70 % of the initial CH_3Cl is consumed in reactions that produce

chloroethane, methane, and other byproducts. The fraction of CH_3Cl remaining decreases with increasing time (Table 4). In longer experiments than those showed here, CH_3Cl was fully destroyed. With increasing extent of CH_3Cl destruction, the δD and δ^{13}C values of the residual CH_3Cl increase relative to their starting values by as much as 150 ‰ in δD and 19 ‰ in δ^{13}C (Table 4).

Unlike δD and δ^{13}C values, which always increase with increasing extent of CH_3Cl destruction, the direction of change in $\Delta_{13_{CH_2D(wg)}}$ depends on the initial value of the gas used, and samples cease changing as reaction time increases (Fig. 8; Table 4). For experiments using the plusD-Cl standard, $\Delta_{13_{CH_2D(wg)}}$ values first increase from –5.44 ‰ ± 0.08 ‰ to 0.42 ± 0.19 ‰ (1 s.e.) after 106 hr of heating and then in a separate experiment remain unchanged (at the ±1 s.e. level) after 185 hours with a value of 0.49 ± 0.19 ‰. For the plus^{13}C-Cl standard, $\Delta_{13_{CH_2D(wg)}}$ values first *decrease* from an initial value of 26.39 ± 0.17 ‰ to 0.59 ± 0.23 ‰ at 90 hr and then in a separate experiment remain unchanged (at the ±1 s.e. level) at 0.34 ± 0.21 ‰ after 120 hr. Finally, in the single experiment using the BI-Cl-1 standard, the mean $\Delta_{13_{CH_2D}}$ value changes from 0.01 ± 0.12 ‰ to 0.44 ± 0.17 ‰ after heating for 104 hr. This change is within ± 2 s.e. of the starting value. In summary, final mean values regardless of initial value or heating duration are 0.458 ± 0.093 (1σ; n = 5) (Fig. 8). Given our typical external reproducibility of ~0.25 ‰ (1σ), these values are statistically indistinguishable. As such final $\Delta_{13_{CH_2D(wg)}}$values are bracketed from two directions and measured values are time invariant. As will be discussed below (Section 9.1), this indicates internal isotopic equilibrium was reached in all experiments.

With the PlusD-Cl-std, $\Delta_{12_{CHD_2(wg)}}$ values decrease from an initial value of 13,382 ‰ to 44.68 ± 2.23 ‰ after 106 hours of heating and in a separate experiment to –4.48 ± 2.46 ‰ after 185 hr of heating (Fig. 9). For the plus^{13}C-Cl-std experiment the $\Delta_{12_{CHD_2(wg)}}$ value decrease from 87.19 ± 2.79 ‰ to 0.14 ± 2.10 ‰ (1 s.e.) after 120 hr of heating. Finally, for the BI-Cl-1 standard, the $\Delta_{12_{CHD_2(wg)}}$ value decreases from 6.06 ± 1.21 ‰ to –2.20 ± 1.81 ‰ (1 s.e.) after 104 hr of heating. Three of these four experiments have a mean value of −2.18 ± 2.31 ‰ (1σ). Given our typical external precision (± 2.25 ‰), these values are statistically indistinguishable. We propose and proceed with the assumption that these three experiments reached internal $\Delta_{12_{CHD_2}}$ equilibrium as they show time invariance despite starting from different values (even though they are not a true bracket). That equilibrium $\Delta_{13_{CH_2D(wg)}}$ values were reached in the same experiments supports this proposal. This assumption, and the explanation for why the shorter PlusD-Cl-std experiment did not fully equilibrate in $\Delta_{12_{CHD_2(wg)}}$, are discussed in Section 9.1.

For completeness, we note that we attempted equilibrations on other catalysts and at different temperatures that ultimately failed due to lack of exchange or destruction of the analyte. For both CH_3Cl and CH_3F, catalysts tried included γ-Al_2O_3, Ni, Pd, and K_2PtCl_4 at temperatures from 25-350 °C (chosen based on previous work showing these activate C–H bonds and lead to isotopic equilibrium; e.g., Goldshleger et al., 1969; Horibe and Craig, 1995; Sattler, 2018). We also attempted to equilibrate CH_3Cl at higher temperatures (750–1000 °C) with no catalyst. Equilibration of CH_3Cl on Pt/Al_2O_3 at 150 °C was attempted, but exchange rates were too sluggish, while at 250 °C and 350 °C we found breakdown outpaced equilibration.

736
737 **8.8 Theoretical calculations of Δ values as a function of temperature**
738 Here we provide the results from our theoretical estimates of the equilibrium temperature
739 dependence of Δ values for methyl groups and methane. Calculated bond lengths and harmonic
740 vibrational frequencies are given in Electronic Annex Table EA5. For CH_3Cl, CH_3F, and CH_4,
741 all C–H bond lengths are the same in a given molecule and thus all Hs are equivalent. For
742 methanol, one of the three C–H bonds is calculated to be shorter than the other two (Table EA5),
743 and thus there are two different types of C–H bonds within methanol with different tendencies to
744 concentrate D vs. H or ^{13}C vs. ^{12}C. Differences in Δ values for these different C–H methanol
745 bonds are smaller than measurement precision: $\Delta_{^{13}CH_2D}$ values for each type of bond differ by ≤
746 0.2‰ at all temperatures ≥ 0 °C; $\Delta_{^{12}CHD_2}$ values for the shorter C–H bond cannot be computed
747 since the methanol methyl group has only one of these, but the $\Delta_{^{12}CHD_2}$ value of just the longer
748 two C–H bonds is within 0.4 ‰ of the $\Delta_{^{12}CHD_2}$ value computed using the geometric mean of all
749 three. Nonetheless, we incorporate these differences into the computed $\Delta_{^{13}CH_2D}$ and
750 $\Delta_{^{12}CHD_2}$ values for methanol by geometrically averaging the RPFR value across all three C–H
751 bonds (Table EA6). Using the arithmetic mean of these RPFRs produces indistinguishable
752 results in Δ values.
753
754 Δ values are calculated with Eqns. 15 and 16 over a temperature range of 0 to 10,000 °C and fit
755 to sixth-order polynomials. Fits to all molecules computed using the various theoretical level and
756 basis set combinations are provided in Table EA7. Polynomial fits match theoretical values
757 within ± 0.01 ‰. The polynomial fit to the equilibrium $\Delta_{^{13}CH_2D}$–T relationship for CH_3Cl at the
758 highest level of theory/basis set used (CCSD/aug-cc-pVTZ) is:
759

$$\Delta_{^{13}CH_2D} = \frac{-1.43373 \times 10^{16}}{T^6} + \frac{1.75779 \times 10^{14}}{T^5} + \frac{-8.13239 \times 10^{11}}{T^4} + \frac{1.63133 \times 10^{9}}{T^3} + \frac{-6.36732 \times 10^{5}}{T^2} + \frac{70.7370}{T} + 3.07841 \times 10^{-3} \quad (17)$$

763 where T is in kelvin. This equation is the basis for our thermodynamic reference frame for
764 $\Delta_{^{13}CH_2D}$ values, reported below.
765
766 The polynomial fit to the equilibrium $\Delta_{^{12}CHD_2}$–T relationship for CH_3Cl at the highest level of
767 theory/basis set used (CCSD/aug-cc-pVTZ) is:
768

$$\Delta_{^{13}CH_2D} = \frac{1.13211 \times 10^{16}}{T^6} + \frac{-8.86159 \times 10^{13}}{T^5} + \frac{1.68048 \times 10^{10}}{T^4} + \frac{1.28883 \times 10^{9}}{T^3} + \frac{-1.15627 \times 10^{6}}{T^2} + \frac{4.24630 \times 10^{2}}{T} - 4.54342 \times 10^{-2} \quad (18)$$

772 where T is in kelvin. As above, this equation is the basis for our thermodynamic reference frame
773 for $\Delta_{^{12}CHD_2}$ values, reported below.
774

Equilibrium $\Delta_{13_{CH_2D}}$ and $\Delta_{12_{CHD_2}}$ values calculated using different levels of theory and basis set differ by < 0.3 ‰ and < 3.0 ‰, respectively, over the entire relevant *T* range 0–10,000 °C (Figs. 10, A10, A11). This is in spite of large differences in individual RPFRs among the different methods and basis sets (Table EA6). For example, calculated RPFRs among all three combinations of theory levels and basis sets are as large as ~5‰ for $^{R-^{13}CH_3}$RPFR and ~60 ‰ for $^{R-^{12}CH_2D}$RPFR.

Equilibrium values of $\Delta_{13_{CH_2D}}$ for CH_3Cl, CH_3F, and CH_3OH are similar to each other and, in turn, similar to analogous $\Delta_{13_{CH_3D}}$ values for methane. For example, for calculations preformed using the highest level of theory and basis set (CCSD/aug-cc-pVTZ), $\Delta_{13_{CH_2D}}$values of the different methyl groups agree within 0.1 ‰ at a given temperature and are within 0.2 ‰ of the analogous $\Delta_{13_{CH_3D}}$ values for methane (Fig. 10c). For the same molecule computed at different levels of theory, $\Delta_{13_{CH_2D}}$ values are within 0.2 ‰ (Fig. A10). Within this range, discrepancies in $\Delta_{13_{CH_2D}}$ values among different levels of theory are systematic across molecules: $\Delta_{13_{CH_2D}}$ values calculated at the MP2 level of theory are always higher than the CCSD values, which are always higher than the B3LYP values (Fig. A10). Differences are highest at low temperatures and decrease as temperatures increase (Figs. 10, A10).

Calculated equilibrium $\Delta_{12_{CHD_2}}$ values for CH_3Cl, CH_3F, and MeOH are always within 0.5 ‰ of each other at the same level of theory from 0 to 10,000 °C (Fig. 10b,d). At a given temperature, $\Delta_{12_{CHD_2}}$ is systematically lower than $\Delta_{12_{CH_2D_2}}$ in methane by about 2–3 ‰ for T < 100 °C and for calculations done at the same level theory (Fig. 10d). For a specific molecule, differences between theoretical $\Delta_{12_{CHD_2}}$ values calculated using the CCSD and MP2 levels of theory (both with the aug-cc-pVTZ basis set) are small (<0.1 ‰; Fig. A11). The corresponding B3LYP curves are systematically lower than the other two by up to 1 ‰ at 0 °C.

The above calculations were performed using the most abundant (or only, for fluorine) stable isotope of the heteroatom attached to the methyl group (i.e., ^{35}Cl, ^{19}F, and ^{16}OH). We investigated the effect of a ^{37}Cl isotope substitution on the equilibrium composition of the methyl group given its relatively high natural abundance (~25%). Temperature dependencies of $\Delta_{13_{CH_2D}}$ and $\Delta_{12_{CHD_2}}$ for $CH_3{}^{35}Cl$ vs. $CH_3{}^{37}Cl$ are within ± 0.01 ‰, and thus choice of the chlorine isotope is unimportant for our calculations.

8.9 A thermodynamic reference frame for $\Delta_{13_{CH_2D}}$ and $\Delta_{12_{CHD_2}}$ measurements

Here we place our Δ values in a thermodynamic reference frame, where 0 ‰ is equivalent to an infinite temperature and positive Δ values can be used to calculate apparent clumped-isotope-based temperatures. To do this, we assume our 200 °C experiments reached internal isotopic equilibrium. These experiments yielded error-weighted mean $\Delta_{13_{CH_2D(wg)}}$ and $\Delta_{12_{CHD_2(wg)}}$ values of 0.452 ± 0.042 and −1.98 ± 1.33 ‰ relative the working reference gas (±1 s.e.) (Section 8.7). As per Eqns. 17, 18 (Section 8.8), theoretical equilibrium $\Delta_{13_{CH_2D}}$ and $\Delta_{12_{CHD_2}}$ values at

200 °C are 2.618 ‰ and 5.46 ‰. The $\Delta_{13_{CH_2D,wg}}$ and $\Delta_{12_{CHD_2,wg}}$ values of our CH_3Cl working gas (CIT-Cl-2) in the thermodynamic reference frame are thus 2.164 ± 0.042 and 7.46 ± 1.33 ‰. With these values, we are able to convert all sample $\Delta_{13_{CH_2D(wg)}}$ and $\Delta_{12_{CHD_2(wg)}}$ values measured relative to the working gas to the thermodynamic reference frame (Sections A1.3, A1.4 and Eqns. A21, A26).

In doing these conversions, we do not propagate the uncertainties on the $\Delta_{13_{CH_2D}}$ and $\Delta_{12_{CHD_2}}$ values of the working gas into equivalent sample values. These uncertainties are systematic and ultimately will not affect relative differences in $\Delta_{13_{CH_2D}}$ and $\Delta_{12_{CHD_2}}$ values among samples measured using the same working gas (as is the case here).

8.10 Clumped isotope compositions of synthetic and wood methyl groups

We compare $\Delta_{13_{CH_2D}}$ and $\Delta_{12_{CHD_2}}$ values of various commercially purchased compounds and environmental wood samples in Fig. 11. Commercially purchased samples include CH_3F and CH_3Cl gases, CH_3I and methanol liquids, and a syringaldehyde powder. The five wood samples are from birch, poplar, bamboo, beech, and tineo trees. All samples are placed into the CH_3Cl thermodynamic reference frame as reported above. Additionally, samples measured as CH_3F are converted to equivalent $\Delta_{13_{CH_2D}}$ values for CH_3Cl based on an offset of 0.479 ‰ as reported above.

Across all commercial and environmental wood samples, we observe a range in $\Delta_{13_{CH_2D}}$ of ~11 ‰ (0 to 11 ‰), and in $\Delta_{12_{CHD_2}}$ of ~50 ‰ (−36 to 13 ‰) (Fig. 11, Table 5). These ranges are ~50 and 20× typical measurement precision, respectively. An immediate observation is that wood methoxyl groups are distinctly different in their $\Delta_{13_{CH_2D}}$ and $\Delta_{12_{CHD_2}}$ values compared to methyl groups from commercial sources (Fig. 11, Table 5). Specifically, wood methoxyl groups are relatively high in $\Delta_{13_{CH_2D}}$ (9.5 to 11.25 ‰ vs. random) and low in $\Delta_{12_{CHD_2}}$ (−8 to −35 ‰ vs. random) compared to the studied commercial compounds, which are relatively low in $\Delta_{13_{CH_2D}}$ (0 to 3‰) and high in $\Delta_{12_{CHD_2}}$ (−5 to 13 ‰).

Differences are also observed between the various commercial compounds (Table 5). CH_3Cl and CH_3F gases have a tight range in $\Delta_{13_{CH_2D}}$ values of 2–3 ‰ (n =4), despite originating from three different suppliers and having 28 and 64 ‰ ranges in $\delta^{13}C$ and δD respectively. The commercial liquids and solids have lower $\Delta_{13_{CH_2D}}$ values than the gases, between 0 and 1.76 ‰ (n = 3). The three commercial liquids also have lower $\Delta_{12_{CHD_2}}$ values than the two CH_3Cl gases (–5 to 2 ‰ vs. 7.5 and 13 ‰).

Assuming that the thermodynamic reference frame for CH_3Cl is a reasonable approximation for non-CH_3Cl compounds (discussed below), $\Delta_{13_{CH_2D}}$ and $\Delta_{12_{CHD_2}}$ values can be converted into 'apparent' equilibrium temperatures using Eqns. 17 and 18. Formation of methyl groups in internal clumped isotopic equilibrium requires that both $\Delta_{13_{CH_2D}}$ and $\Delta_{12_{CHD_2}}$ yield the same (within error) temperature (e.g., Yeung 2012; Young et al., 2017). Such a line of mutual

equilibrium is given in Figure 12. Alternatively, kinetic isotope effects associated with methyl group formation or breakdown, or mixing of different methyl-group sources can yield non-equilibrium Δ values (e.g., Stolper et al., 2015; Wang et al., 2015; Yeung et al., 2015; 2017; Young et al., 2017), including negative values. Negative Δ values cannot occur in isotopically equilibrated systems and necessarily reflect non-equilibrium processes.

The apparent equilibrium $\Delta_{13_{CH_2D}}$ temperatures of commercial synthetic gases are all between 175 and 250 °C: 178 and 194 °C for CH_3F and 244, and 247 °C for CH_3Cl (errors of ± 10 to 25 °C, 1 s.e.; Table 5). The apparent $\Delta_{13_{CH_2D}}$ temperatures of our commercial syringealdehyde, methanol, and iodomethane samples are ~300, ~450, and >1000 °C, respectively (Table 5). Of five commercial compounds also measured for $\Delta_{12_{CHD_2}}$, only the methanol data point intersects (within 2 s.e.) the line of mutual equilibrium (Fig. 12). Specifically, the methanol has apparent equilibrium temperatures of 448 $^{+43}/_{-36}$ °C for $\Delta_{13_{CH_2D}}$ and 353 $^{+inf}/_{-163}$ °C for $\Delta_{12_{CHD_2}}$ (±1 s.e.). In contrast, the two CH_3Cl gases have apparent equilibrium $\Delta_{12_{CHD_2}}$ temperatures that are colder than their $\Delta_{13_{CH_2D}}$ temperatures: 150 $^{+31}/_{-25}$ °C and 67 $^{+14}/_{-13}$ °C for $\Delta_{12_{CHD_2}}$ vs. ~245 ± ~12 °C for $\Delta_{13_{CH_2D}}$. $\Delta_{12_{CHD_2}}$ values of the syringaldehyde and CH_3I stds are both < 0 ‰ and thus cannot yield apparent temperatures.

Measured $\Delta_{13_{CH_2D}}$ and $\Delta_{12_{CHD_2}}$ values of wood methoxyl groups reflect non-equilibrium isotopic compositions (Figs. 11, 12). Specifically, the wood methoxyl $\Delta_{12_{CHD_2}}$ values from the three examined specimens are < 0 ‰ and as low as −35 ‰, which cannot occur in an equilibrated system. The expected equilibrium $\Delta_{13_{CH_2D}}$values for typical earth surface temperatures (0–30 °C) are 5.75 to 6.75 ‰, whereas the wood methoxyl $\Delta_{13_{CH_2D}}$ values from the five examined specimens are between 9.5 ‰ and 11.25 ‰ (n = 5 samples, n = 12 total replicates). These values correspond to apparent equilibrium temperatures of −55 to −80 °C, also indicating non-equilibrium clumped isotopic compositions (note these temperatures were calculated using RPFRs—eqns. 14 and 15—not by extrapolating the polynomial fit in eqn. 17). As above, this comparison assumes that the equilibrium $\Delta_{13_{CH_2D}}-T$ relationship in CH_3Cl is equivalent to that of the molecular form in which these methoxyl groups are originally synthesized in trees. This assumption is discussed below.

9. Discussion

9.1 Precision and accuracy of methyl group isotopic measurements

Here we discuss the precision and accuracy of our isotopic measurements of methoxyl groups. The critical observation for our purposes is that observed external precisions on replicate analyses for $\Delta_{13_{CH_2D}}$ and $\Delta_{12_{CHD_2}}$ are similar to internal measurement precision regardless of the analyte type: CH_3F and CH_3Cl gases, CH_3I, and methoxyl-containing compounds all have 1σ external precisions on replicates of 0.09–0.39 ‰ vs. mean internal s.e. of 0.25 ‰ for $\Delta_{13_{CH_2D}}$; 2.50 ‰ external vs. 2.45 ‰ internal for $\Delta_{12_{CHD_2}}$. Although external precision for δD and δ^{13}C measurements is similar to internal precision for CH_3F and CH_3Cl standards (~0.14 and 0.01 ‰, respectively), external δD and δ^{13}C precision on replicates decreases for samples that require derivatization steps, to ~0.5 to 2 ‰. The decrease in precision is likely due incomplete recovery

during the chemical reactions or fractionations associated with gas handling or purification. We interpret this to indicate that the processes that decrease precision for δD and δ^{13}C determinations are mass-dependent such that they largely cancel when Δ values are determined. Such is also the case for clumped isotope (e.g., Huntington et al., 2009) as well as triple oxygen isotope (e.g., Miller et al., 2002) and quadruple sulfur isotope (e.g., Ono et al., 2006) measurements.

The CH_3F analyses were acquired over the course of 6 months and CH_3Cl analyses over 9 months. Over this time frame we observe no trends vs. time for any δ or Δ measurements of gas standards (e.g., Fig. 3). These time frames span instances of instrument maintenance (e.g., filament and high-resolution slit replacement). Additionally, between analytical sessions, methane was analyzed on the same instrument with a different set of bellows. This demonstrates that Δ values are stable and precise at the reported level of measurement uncertainty on timeframes of at least many months.

Comparisons of δ^{13}C values on standards with published isotopic compositions indicate that our measurements are accurate to within the precision indicated by replicate analyses (Fig 6). For δD, although relative differences are recovered between labs (Fig. 5c), there is a systematic offset in δD of –18 ± 6 ‰ (1σ; n = 3) between our values and those reported in Greule et al. (2019) (Fig. 5b). One source of this offset could be isotopic fractionation of our CH_3F and CH_3Cl reference gases during offline combustion + reduction at Indiana U. Specifically, following the measurement of our reference gases at Indiana U., it was found that off-line δD determinations of organohalogen compounds can differ from those measured using continuous flow systems with chromium reactors added to achieve high (> 96 %) yields (Gehre et al., 2017). This was especially problematic for chlorinated hydrocarbons with high molar Cl/H ratios (≥ 1) and low H_2 yields (78–82 %) (Gehre et a., 2017). However, CH_3Cl has a molar Cl/H ratio of 0.33 and H_2 yields from its reductions were 95–96 %. For compounds with similar Cl/H ratios and δD values as our CH_3Cl reference gas, δD offsets between off-line vs on-line continuous flow values were 1 to 8 ‰ (Gehre et al., 2017), which are similar in magnitude to differences observed between the same laboratories and methods for non-halogenated organic standards (±1 to 9 ‰; Schimmelmann et al., 2016). Nonetheless, some disagreement (order 10 ‰) between our δD measurements and those of Greule et al. (2019) may be associated with our use of an off-line conversion vs. their use of the specialized on-line chromium reduction system for calibration. Likewise, the better agreement between our δD measurements and those of Lee et al. (2019) could be because both labs are anchored to standards measured at Indiana U.

Regardless of the exact source of these disagreements, the critical points for our purposes are: (*i*) any inaccuracy in the δD composition of our working gases has no effect on our $\Delta_{^{13}CH_2D}$ and $\Delta_{^{12}CHD_2}$ determinations. For example, changing the working gas δD composition by 20 ‰ changes calculated $\Delta_{^{13}CH_2D(wg)}$ and $\Delta_{^{12}CHD_2(wg)}$ values by < 0.0001 ‰ and < 0.002 ‰, respectively. And, (*ii*) the derivatization methods developed here, though extensive, do not detectably fractionate δD nor δ^{13}C values. However, these results do indicate that direct comparison of methoxyl δD values made by different methods in different laboratories may be problematic.

Assessing the accuracy of $\Delta_{^{13}CH_2D}$ and $\Delta_{^{12}CHD_2}$ values in a thermodynamic reference frame requires (*i*) determining the Δ value of the working gas in the thermodynamic reference frame and (*ii*) demonstrating that actual vs. measured differences in Δ values are equal (i.e., measurement linearity is 1.0). The usual way to demonstrate both is to equilibrate samples at a range of temperatures and verify that measured differences between Δ values are equal to expected differences based on theory, or perform a correction based on the observed offsets (Dennis et al., 2011; Stolper et al., 2014b; Yeung et al., 2016; Young et al., 2017; Popa et al., 2018; Eldridge et al., 2019). We were able to equilibrate various CH_3Cl gases at 200 °C, as shown by attaining time-invariant coalescence in Δ values despite different starting values and, in the case of $\Delta_{^{13}CH_2D}$, bracketing. However we were unable to equilibrate CH_3Cl at multiple temperatures and so we cannot conduct this test to show measurement accuracy.

Nonetheless, we propose that measured vs. actual differences in $\Delta_{^{13}CH_2D}$ and $\Delta_{^{12}CHD_2}$ values between samples are equivalent for the following reasons: (*i*) Eldridge et al. (2019) demonstrated that samples of methane equilibrated from 1 to 500 °C and measured on the same instrument with the same detectors used here agree 1:1 with theoretical predictions. This indicates that the instrument and detectors used here for a similar ion (CH_4^+ vs CH_3^+) exhibit a linearity of 1.0. (*ii*) A linearity different from 1.0 can cause Δ values of samples equilibrated at the same temperature to vary as a function of bulk isotopic composition (Huntington et al., 2009; Dennis et al., 2011). The samples we equilibrated at 200 °C yield the same $\Delta_{^{13}CH_2D(wg)}$ and $\Delta_{^{12}CHD_2(wg)}$ values despite ranges in δD and δ^{13}C of 140 and 45 ‰ (Fig. 8b, 9b). As Δ values are derived from differences between measured $\delta^{13}CH_2D$ or $\delta^{12}CHD_2$ values vs. $\delta^{13}CH_3$ and $\delta^{12}CH_2D$ values, the lack of a dependence of Δ vs. δD or δ^{13}C indicates a measurement linearity of 1.0. (*iii*) Differences between samples measured as either CH_3F or CH_3Cl are 1:1 over an 11 ‰ range in $\Delta_{^{13}CH_2D}$, and a range in $\delta^{13}CH_2D$ of ~250 ‰. This demonstrates that our measurements of relative differences in $\Delta_{^{13}CH_2D}$ values from methyl fragments are insensitive to chlorination vs. fluorination of CH_3I and subsequent mass spectrometric measurement conditions such as differences in source chemistry, source pressures, tuning conditions, fragmentation and adduction rates, ion beam intensities, etc. (*iv*) Finally, we analyzed the plusD-Cl standard at 40 % of typical source pressure, resulting in 40 % of typical methyl fragment ion intensities. Despite this change in instrument conditions, measured values are indistinguishable (within ± 1 s.e.) in δD, δ^{13}C, and $\Delta_{^{13}CH_2D}$ from the long-term mean values acquired under normal measurement conditions (Table EA1). Based on the above tests, we conclude that measured vs. actual differences in Δ values are indistinguishable, and thus that our Δ measurements are accurate.

The elevated $\Delta_{^{12}CHD_2(wg)}$ of the 106 hour experiment (44.68 ‰) relative to values obtained over similar time frames in other experiments (0.14 to −4.48 ‰) is likely the result of this sample starting with an exceptionally enriched $\Delta_{^{12}CHD_2(wg)}$ value (13,382 ‰). Assuming −2.18 ‰ is the equilibrium value at 200 °C, a measured value of 44.68 ‰ indicates this experiment was 99.7 % equilibrated. Such small deviations from equilibrium (<0.3 ‰ deviation) would not be detectable for other samples given their starting $\Delta_{^{12}CHD_2(wg)}$ values and our typical precision (± 2–3 ‰).

One complexity with these experiments we now discuss is potential issues associated with our removal of chloroethane (C_2H_5Cl). During equilibrations of CH_3Cl on Pt/Al_2O_3, chloroethane (C_2H_5Cl) was generated. It was removed via pyrolysis at 500 °C (not in the presence of the catalyst). Due to the high temperatures and potentially reactive decomposition products involved, we consider whether this procedure could affect measured CH_3Cl Δ values. We examined this issue as follows: First, we heated pure CH_3Cl from the plusD-Cl-std at 500 °C for 15 min and purified it identically as the pyrolysis experiments. Recovery was 100 ± 2 %. $\delta^{13}C$, δD, and $\Delta_{^{13}CH_2D(wg)}$ values changed by <0.1, 0.02, and 0.1 ‰ respectively. The $\Delta_{^{12}CHD_2(wg)}$ value (determined by measuring peak heights due to the enrichments) before and after heating were 13,382 ‰ and 13,508‰, which we consider indistinguishable. This shows that heating pure CH_3Cl at 500 °C for tens of minutes does not result in either breakdown or changes in isotopic composition.

Second, although pure CH_3Cl is resistant to isotopic alteration at 500 °C for tens of minutes, hydrogen exchange reactions with either C_2H_5Cl or its decomposition products could occur that partially or wholly internally isotopically equilibrate CH_3Cl at 500 °C. However, complete or partial equilibration at 500 °C is inconsistent with the experiments performed on plusD-Cl-std with initial $\Delta_{^{12}CHD_2(wg)}$ values of 13,382 ‰. As reported above, samples equilibrated at 200 °C for 106 vs 185 hours yield a difference in $\Delta_{^{12}CHD_2(wg)}$ of 49.16 ‰, despite being heated at 500 °C for identical lengths of time. If significant exchange of CH_3Cl with C_2H_5Cl or its decomposition products occurred at 500 °C, we would not expect this difference to be preserved.

Based on these tests and observations, we have proposed and proceeded with the assumption that pyrolysis of C_2H_5Cl at 500 °C did not affect Δ values of CH_3Cl and that internal isotopic equilibrium at 200 °C was achieved.

9.2 Choice of CH_3F vs. CH_3Cl, and application to other methyl-bearing compounds

Above we demonstrated that external precisions for δD, $\delta^{13}C$, and $\Delta_{^{13}CH_2D}$ are equivalent for CH_3F and CH_3Cl and that relative differences in δD, $\delta^{13}C$, and $\Delta_{^{13}CH_2D}$ values between samples measured as CH_3F vs. CH_3Cl are 1:1. As such, both are viable analytes for methoxyl clumped-isotope measurements. For ongoing work, we have elected to use CH_3Cl exclusively because: (*i*) For equivalent sample sizes, CH_3Cl yields 4× higher sensitivity allowing $\Delta_{^{13}CH_2D(wg)}$ to be measured at the same precision in half the time as CH_3Cl vs. as CH_3F. (*ii*) CH_3Cl provides sufficient sensitivity to allow measurement of $\Delta_{^{12}CHD_2}$. (*iii*) The chlorination chemistry yields fewer contaminants (e.g., NH_2^+, SiF_4 and CH_2F_2 during fluorination), is safer and, in our experience, easier to perform.

We note that because our mass spectrometric procedure only uses isotope ratios of methyl fragment ions, it is agnostic of the source of these ions. I.e., the analytical methods for measuring δD, $\delta^{13}C$, and $\Delta_{^{13}CH_2D}$ values of methyl groups in CH_3Cl and CH_3F differ only in the source tuning conditions (used to maximize methyl fragment ion production in each analyte) and the absolute intensities of methyl ion beams. As we have shown that relative differences in $\Delta_{^{13}CH_2D}$ values for measurements using these two analytes are indistinguishable, this suggests that our mass spectrometric measurement could be similarly applicable to other sources of methyl

fragment ions beyond CH_3Cl and CH_3F. Thus, the analytical procedures described here could be adopted with minimal modification to determine the position-specific δD and δ^{13}C, and clumped ^{13}C–D and D–D compositions of methyl groups from other methyl-containing molecules of geochemical interest, such as methyl amines, methyl sulfides, and simple *n*-alkanes.

9.3 On the use of a uniform thermodynamic reference frame

We have placed all our measurements in a thermodynamic reference frame based on the equilibrium clumped isotopic composition of CH_3Cl. This approach assumes that it is appropriate to compare measurements of methanol, CH_3F, CH_3I, syringaldehyde, or wood in a thermodynamic reference frame based on CH_3Cl. This assumption is supported by the observation that theoretical calculations of $\Delta_{^{13}CH_2D}$ and $\Delta_{^{12}CHD_2}$ values in CH_3F, CH_3Cl, and CH_3OH agree within 0.2 and 0.5 ‰ (respectively) over a range of 0 to 10,000 °C (Fig. 10), regardless of theoretical level and basis set size. That Δ values are largely independent of theoretical level used is consistent with previous observations that errors in RPFR determinations are nearly perfectly canceled when Δ values are calculated (Webb and Miller, 2013; Eldridge et al., 2019). The present work indicates that for methyl groups, $\Delta_{^{13}CH_2D}$ and $\Delta_{^{12}CHD_2}$ values are also largely independent of the bonding partner and all methyl groups can be considered together. This was also found in previous calculations of equilibrium $\Delta_{^{13}CH_2D}$ clumping in methanol, methanethiol (CH_3SH) and acetate (CH_3COOH) at 25 °C , which agreed within 0.3‰ (Wang et al., 2015). Our predictions at 25 °C are systematically lower than theirs by 0.2–0.5 ‰. Nonetheless, this suggests that methyl group clumping in the gas phase is insensitive to the bonding partner at the level of our measurement precision (~0.25‰), and that the CH_3Cl-based reference frame is a reasonable approximation for that of biologic methyl groups such as methoxyl groups in wood. However, future theoretical work on more complex molecules (such as lignin precursors) will be needed to evaluate this assumption.

9.4 Sources and implications of isotopic clumping in commercial and environmental methyl groups

Based on this initial data set, $\Delta_{^{13}CH_2D}$ and $\Delta_{^{12}CHD_2}$ values appear to differ systematically between commercial compounds and environmental woods (Fig. 11). These differences probably arise due to isotope effects associated with differing methyl group synthesis pathways. For example, methyl groups in many commercial compounds are derived from methanol, which is primarily synthesized at industrial scales from H_2, CO, and CO_2 on metal catalysts at elevated temperatures (>200 °C) (e.g., Ott et al., 2012). In contrast, methyl groups in wood lignin are formed by a series of enzyme-catalyzed biosynthetic steps (e.g., Schmidt et al., 2015). Regardless of the cause, this limited data set indicates promise for forensic applications of $\Delta_{^{13}CH_2D}$ and $\Delta_{^{12}CHD_2}$ measurements for the identification of natural vs. commercial (and likely synthetic) methyl group sources.

9.4.1 Sources of $\Delta_{^{13}CH_2D}$ and $\Delta_{^{12}CHD_2}$ values in methyl groups in commercial materials

Commercial materials yield apparent $\Delta_{^{13}CH_2D}$-based temperatures between 175 °C and infinity. For commercial materials with positive $\Delta_{^{12}CHD_2}$ values, apparent $\Delta_{^{12}CHD_2}$-based temperatures range from 70 °C to ~350 °C. However, some commercial samples have negative $\Delta_{^{12}CHD_2}$ values that do not correspond to any temperature. We now speculate on the cause of these isotopic

variations. To do this, we first consider the conditions in which these methyl groups were likely formed. Methanol is the principal source of methyl groups for the synthesis of methyl halogens and organic monomers (Cheng, 1994; Ott et al., 2012; Siegemund et al., 2016; Ohligschläger et al., 2019). Since the 1960s, industrial methanol has been produced by the reaction of H_2, CO_2, and CO on Cu–ZnO–Al_2O_3 catalysts at temperatures between 200 and 300 °C. These catalyzed reactions proceed to chemical equilibrium (Cheng et al., 1994; Ott et al., 2012) and thus could result in isotopic equilibrium if sufficient exchange reactions occur on the catalyst. However, during industrial methanol production, high conversion yields (>80 %) are obtained by extracting the produced methanol and recycling residual gases back through the reactor (Ott et al., 2012). Thus, clumped-isotope effects associated with mixing may also play a role. Finally, isotope effects associated with the transfer of the methyl group to F, Cl, I or another substrate must also be considered if this transfer is not quantitative or if C-H isotope exchange reactions occur along with the transfer.

The methanol standard is the only sample examined that yields apparent equilibrium temperatures for $\Delta_{13_{CH_2D}}$ and $\Delta_{12_{CHD_2}}$ within error of each other (448 $^{+43}/_{-36}$ °C and 353 $^{+inf}/_{-162}$ °C respectively). However, the $\Delta_{13_{CH_2D}}$-based temperaure, which has the smaller error, is at least 150 °C higher than would be expected given its likely synthesis conditions (200–300 °C). This may indicate that isotopic equilibrium is not reached during methanol generation over catalysts. If correct, then the clumped isotopic composition of the methanol signature could represent a process of partial equilibration. Alternatively, isotope effects associated with transport, storage, or nonlinear mixing could also cause disequilibrium signatures.

The tight range of $\Delta_{13_{CH_2D}}$-derived temperatures from the CH_3Cl and CH_3F gases (175-250 °C), despite ~65 ‰ and 30 ‰ ranges in δD and δ^{13}C, could be consistent with these methyl groups having attained clumped isotope equilibrium during formation at 200–300 °C during methanol synthesis. Formation in complete internal isotopic equilibrium, however, is inconsistent with measured $\Delta_{12_{CHD_2}}$ values, which are 3 and 10 ‰ higher than the mutual equilibrium line. Post-formation processes such as non-linear mixing could explain this discrepancy, since these are expected to affect $\Delta_{12_{CHD_2}}$values more strongly than $\Delta_{13_{CH_2D}}$ (Eiler, 2013; Taenzer et al., 2020). In any case, the lack of mutual equilibrium, plus the single observation that methanol (i.e., the proposed methyl group precursor) has a different apparent equilibrium temperature, suggests a formation pathway more complicated than a single, batch equilibration for these synthetic methyl groups.

The CH_3I std has a $\Delta_{13_{CH_2D}}$ value indistinguishable from the random distribution (which occurs at infinite temperature) and a negative $\Delta_{12_{CHD_2}}$ value, and thus its isotopic composition also cannot reflect formation in internal isotopic equilibrium. Similarly, although the syringaldehyde $\Delta_{13_{CH_2D}}$ temperature is compatible with the model for equilibrium methanol synthesis between 200 and 300 °C (295 $^{+50}/_{-41}$ °C), the $\Delta_{12_{CHD_2}}$ value is negative.

Based on this limited examination, it appears that commercial standards are generally out of mutual $\Delta_{13_{CH_2D}}$ and $\Delta_{12_{CHD_2}}$ equilibrium. This disequilibrium may arise partly during methanol

synthesis and partly during transfer to later products (although more synthetic methanol samples must be analyzed to verify this).

9.4.2 Implications of the Δ values of synthetic methyl groups for clumped-isotope compositions of biogenic methane

Regardless of the cause, an important implication of the above observations is that methanol and other commercial methyl-bearing species carry with them distinct clumped isotopic signatures that are lower in $\Delta_{^{13}CH_2D}$ than environmental methyl groups in wood, and often lower than what their likely formation temperatures would predict. This matters as previous studies of the methane clumped isotope compositions of methylotrophic methanogens have used commercially purchased methanol and acetate as substrates in pure cultures and observed that the generated methane is (*i*) generally lower in $\Delta_{^{13}CH_3D}$ and $\Delta_{^{12}CH_2D_2}$ values than methane from hydrogenotrophic methanogens (H_2 + CO_2), and (*ii*) always lower than expected for equilibrium (Stolper et al., 2015; Wang et al., 2015; Douglas et al., 2016; Young et al., 2017; Gruen et al., 2018; Giunta et al., 2019; Douglas et al., 2020). The possibility that differences in these results is due in part to inheritance of clumped isotopic signatures from the methyl substrate has been discussed (Wang et al., 2015; Douglas et al., 2016; Gruen et al., 2018; Giunta et al., 2019), but has been difficult to assess. The methanol measured here, which is the same methanol used in some previous methanogen cultures with measured methane clumped-isotope compositions (Douglas et al., 2016; 2020), is low in Δ values relative to low-temperature equilibrium (1 vs. 6 ‰ in $\Delta_{^{13}CH_2D}$; 3.5 vs. 20 ‰ in $\Delta_{^{12}CHD_2}$). If other commercial methyl substrates are similarly low, this could be an important contribution to the low $\Delta_{^{13}CH_3D}$ and $\Delta_{^{12}CH_2D_2}$ values (vs. equilibrium) observed in methylotrophic methanogen culture experiments. Regardless, measurement of clumped isotope compositions of methyl precursors used in methanogen clumped-isotope experiments has the potential to aid in interpreting what processes the clumped isotopes of microbial methane reflect.

9.4.3 Sources of clumped isotope compositions of wood methoxyl groups

$\Delta_{^{13}CH_2D}$ and $\Delta_{^{12}CHD_2}$ values of wood methoxyl groups are out of internal isotopic equilibrium, but in different directions. Non-equilibrium Δ values in biological systems have been observed for methane, O_2, N_2O, and N_2, and are thus a common feature of biological systems. These non-equilibrium compositions are commonly ascribed to kinetic isotope effects associated with enzymatic reactions (Stolper et al., 2015; Wang et al., 2015; Yeung et al., 2015; Douglas et al., 2016; 2017; Wang et al., 2016; Magyar, 2017, Young et al., 2017; Gruen et al. 2018; Yeung et al., 2019; Ash et al., 2020). It is thus possible and perhaps likely that the observed depletions in $^{12}CHD_2$ and enrichments in $^{13}CH_2D$ result from a combination of multiple enzymatic kinetic isotope effects associated with the synthesis of methyl groups in lignin precursors, reservoir effects associated with use of methyl group components for different biosynthetic processes, and commitment of different precursor sources to lignin methoxyl groups. Despite these potential complexities, the $\Delta_{^{13}CH_2D}$ values in wood are relatively uniform. This suggests that the process (or processes) imparting these isotope effects is shared by trees spanning a range of species (e.g., bamboo to birch) and growing conditions (subtropical to boreal), and thus reflects a basal metabolic process. This being said, within this population of high wood methoxyl $\Delta_{^{13}CH_2D}$ values, the variation in specific organisms is ~7× greater than measurement uncertainty. This

suggests that although a shared process results in $\Delta_{13}{}_{CH_2D}$ values uniformly higher than equilibrium, there are differences in the details of this process among different trees that are reflected in the differences in $\Delta_{13}{}_{CH_2D}$ values in wood. Understanding the controls on these differences will require future studies both in controlled experimental settings such as greenhouses and surveys of environmental samples from different species and environments.

Compared to $\Delta_{13}{}_{CH_2D}$ values, $\Delta_{12}{}_{CHD_2}$ values are all negative and more highly variable, at least 10× greater than measurement uncertainty. These observations may reflect the increased sensitivity of clumped isotope variables involving multiple deuterium substitutions to alteration via avenues such as nonlinear mixing (e.g., Eiler, 2013), combinatorial effects (Yeung et al., 2015), and kinetic isotope effects involving the formation and breakage of C–H bonds (e.g., Young et al., 2017). Considering what is known of the formation pathway of lignin methoxyl groups (e.g., Keppler et al., 2007; Schmidt et al., 2015), all three of these factors may influence the sign and variability of $\Delta_{12}{}_{CHD_2}$ values in wood.

10. Summary and conclusions

We presented measurements of the clumped isotopic compositions of methyl groups derived from a variety of commercial and environmental samples and calculations of equilibrium methyl clumping as a function of temperature. The summary and conclusions of this study are:

- We present methods for the measurement of δD, δ^{13}C, $\Delta_{13}{}_{CH_2D}$, of CH_3F and δD, δ^{13}C, $\Delta_{13}{}_{CH_2D}$, and $\Delta_{12}{}_{CHD_2}$ of CH_3Cl on methyl fragments via isotope-ratio mass spectrometry. Long-term (1.5 yr total) external precisions of gas standards are < 0.2 and 0.03 ‰ (1σ) for δD and δ^{13}C measurements and 0.25 and 2.5 ‰ (1σ) for $\Delta_{13}{}_{CH_2D}$ and $\Delta_{12}{}_{CHD_2}$ measurements. Differences between clumped isotope compositions of samples measured as CH_3F or CH_3Cl follow a slope of 1, indicating measurements are relatively accurate and independent of the specific analyte.

- We propose that our mass spectrometric techniques are generally applicable to the measurement of the singly substituted and clumped isotopic compositions of methyl groups from other gaseous analytes. These could include low molecular weight *n*-alkanes such as ethane and propane and other methyl-bearing volatile organic compounds such as dimethyl sulfide and methanethiol.

- We present methods to extract and derivatize methoxyl groups from synthetic monomers and woods as either CH_3F or CH_3Cl. Reproducibility of δD and δ^{13}C for these extractions are ± 2.0 and 1.5 ‰ or better (1σ). Based on comparisons to standards, δD and δ^{13}C measurements are accurate. External reproducibility for $\Delta_{13}{}_{CH_2D}$ values on these materials match internal measurement precisions of ~0.25 ‰ (1σ). Based on replicate conversions of a CH_3I standard, external reproducibility of $\Delta_{12}{}_{CHD_2}$ values also matches internal measurement precision (~2.5 ‰).

•We equilibrated the clumped isotopic composition of CH_3Cl using a Pt catalyst at 200 °C. These experiments are used to place our measurements of both $\Delta_{13_{CH_2D}}$ and $\Delta_{12_{CHD_2}}$ onto a thermodynamic reference frame that is independent of the clumped isotopic composition of our laboratory's working reference gases.

• We provide theoretical computations for the equilibrium temperature dependence of $\Delta_{13_{CH_2D}}$ and $\Delta_{12_{CHD_2}}$ for chloromethane, fluoromethane, and methanol. Differences in calculated clumped isotope compositions of these various molecules at a given temperature vary by less than 0.2 ‰ for $\Delta_{13_{CH_2D}}$ and 0.5 ‰ for $\Delta_{12_{CHD_2}}$ (temperature range of 0 to 10,000 °C). Because these differences are smaller than measurement precision, we propose that our measurements of Cl-, F-, and O-bound methyl groups can be compared using the same thermodynamic reference frame. Here we use the reference frame defined by equilibrium clumping in CH_3Cl as this is the compound used in our equilibration experiments.

• Systematic differences exist between the clumped isotope compositions of methyl groups from an initial survey of commercial compounds vs. woods. This suggests that $\Delta_{13_{CH_2D}}$ and $\Delta_{12_{CHD_2}}$ values can be used to distinguish methyl group origins even among samples that overlap in δD and δ^{13}C. It also suggests that inheritance of isotopic clumping in commercial methyl group substrates could influence the isotopic clumping of methane from methylotrophic methanogen culture experiments.

•$\Delta_{13_{CH_2D}}$ values from commercial compounds are restricted to a range at or within ~2 ‰ of apparent equilibrium of their likely formation temperatures. $\Delta_{12_{CHD_2}}$ values from the same samples are more scattered, mostly lying 5–10 ‰ above or below the line of mutual equilibrium. These discrepancies likely result from non-equilibrium processes associated with mixing and kinetic isotope effects during industrial-scale synthesis of methyl groups; $\Delta_{12_{CHD_2}}$ values are expected to be more sensitive to such processes.

•The clumped isotope compositions of wood methoxyl groups are distinctively elevated in $\Delta_{13_{CH_2D}}$ and depleted in $\Delta_{12_{CHD_2}}$relative to equilibrium. Wood methoxyl groups are thus out of equilibrium with respect to both parameters but in opposite directions. The relative uniformity of these $\Delta_{13_{CH_2D}}$ and (to a lesser extent) $\Delta_{12_{CHD_2}}$ compositions suggests a shared process by which methoxyl groups are formed in all the trees we measured. The variance within these populations suggests that differences in the details of this process are expressed in the clumped isotope compositions of wood methoxyl groups.

11. Acknowledgements

This project began during MKL's PhD thesis under the intellectual direction of John Eiler and Alex Sessions (Caltech) and we thank them for their support and encouragement. We are grateful to Arndt Schimmelmann (Indiana U.) for calibrating our fluoromethane and chloromethane reference tanks, and to James Farquhar (U. Maryland) for support. We acknowledge advice and input from Todd Dawson and Seth Finnegan (UC Berkeley). We thank Frank Keppler and Marcus Greule (Heidelberg U.), and Sarah Feakins (USC) for providing wood standards and

helpful suggestions during the development of this technique. We additionally thank Gareth Izon (MIT), Hyejung Lee (USC), Ben Passey (U. Mich), Camilo Ponton (WWU), Don Tilley (UC Berkeley), David Wang (ExxonMobil), and Hao Xie (Caltech) for helpful discussions and methodological suggestions. We thank Associate Editor Shuhei Ono, Laurence Yeung and two other anonymous reviewers for constructive feedback that substantially improved the manuscript. MKL acknowledges support from the Agouron Institute Geobiology Postdoctoral Fellowship. DAS and DLE acknowledge support from the Laboratory Directed Research and Development Program of Lawrence Berkeley National Laboratory under U.S. Department of Energy Contract No. DE-AC02-05CH11231. The 253 Ultra Mass Spectrometer was funded by the Heising-Simons Foundation and the University of California, Berkeley.

12. References

Aboul-Gheit, A.K., Cosyns, J., 1976. Activation of platinum-alumina catalysts for the hydrogenation of aromatic hydrocarbons. *J. Appl. Chem. Biotechnol.* **26**, 15–22. https://doi.org/10.1002/jctb.5020260104

Aigueperse, J., Mollard, P., Devilliers, D., Chemla, M., Faron, R., Romano, R., Cuer, J.P., 2000. Fluorine Compounds, Inorganic, in: *Ullmann's Encyclopedia of Industrial Chemistry*. American Cancer Society. https://doi.org/10.1002/14356007.a11_307

Anhäuser, T., Greule, M., Polag, D., Bowen, G.J., Keppler, F., 2017. Mean annual temperatures of mid-latitude regions derived from δ^2H values of wood lignin methoxyl groups and its implications for paleoclimate studies. *Sci. Total Environ*. **574**, 1276–1282. https://doi.org/10.1016/j.scitotenv.2016.07.189

Ash, J.L., Hu, H., Yeung, L.Y., 2020. What Fractionates Oxygen Isotopes during Respiration? Insights from Multiple Isotopologue Measurements and Theory. *ACS Earth Space Chem.* **4**, 50–66. https://doi.org/10.1021/acsearthspacechem.9b00230

Baker, L., Franchi, I.A., Maynard, J., Wright, I.P., Pillinger, C.T., 2002. A technique for the determination of $^{18}O/^{16}O$ and $^{17}O/^{16}O$ isotopic ratios in water from small liquid and solid samples. *Anal. Chem*. **74**, 1665–1673.

Becke, A.D., 1993. Density-functional thermochemistry. III. The role of exact exchange. *J. Chem. Phys.* **98**, 5648–5652. https://doi.org/10.1063/1.464913

Berman, H.M., Westbrook, J., Feng, Z., Gilliland, G., Bhat, T.N., Weissig, H., Shindyalov, I.N., Bourne, P.E., 2000. The Protein Data Bank. *Nucleic Acids Res*. **28**, 235–242. https://doi.org/10.1093/nar/28.1.235

Bigeleisen, J., Mayer, M.G., 1947. Calculation of Equilibrium Constants for Isotopic Exchange Reactions. *J. Chem. Phys*. **15**, 261. https://doi.org/10.1063/1.1746492

Cheng, W.-H., 1994. *Methanol Production and Use.* CRC Press.

Clog, M., Lawson, M., Peterson, B., Ferreira, A.A., Neto, E.V.S., Eiler, J.M., 2018. A reconnaissance study of ^{13}C-^{13}C clumping in ethane from natural gas. *Geochim. Cosmochim. Acta* **223**, 229–244. https://doi.org/10.1016/j.gca.2017.12.004

Comas-Vives, A., Schwarzwälder, M., Copéret, C., Sautet, P., 2015. Carbon–Carbon Bond Formation by Activation of CH_3F on Alumina. *J. Phys. Chem. C* **119**, 7156–7163. https://doi.org/10.1021/jp512598p

Dennis, K.J., Affek, H.P., Passey, B.H., Schrag, D.P., Eiler, J.M., 2011. Defining an absolute reference frame for 'clumped' isotope studies of CO2. *Geochim. Cosmochim. Acta* **75**, 7117–7131. https://doi.org/10.1016/j.gca.2011.09.025

Douglas, P.M.J., Moguel, R.G., Anthony, K.M.W., Wik, M., Crill, P.M., Dawson, K.S., Smith, D.A., Yanay, E., Lloyd, M.K., Stolper, D.A., Eiler, J.M., Sessions, A.L., 2020. Clumped Isotopes Link Older Carbon Substrates with Slower Rates of Methanogenesis in Northern Lakes. *Geophys. Res. Lett*. **47**, e2019GL086756. https://doi.org/10.1029/2019GL086756

Douglas, P.M.J., Stolper, D.A., Eiler, J.M., Sessions, A.L., Lawson, M., Shuai, Y., Bishop, A., Podlaha, O.G., Ferreira, A.A., Neto, E.V.S., Niemann, M., Steen, A.S., Huang, L., Chimiak, L., Valentine, D.L., Fiebig, J., Luhmann, A.J., Seyfried Jr, W.E., Etiope, G., Schoell, M., Inskeep, W.P., Moran, J.J., Kitchen, N., 2017. Methane clumped isotopes: Progress and potential for a new isotopic tracer. *Org. Geochem*. **113**, 262–282. https://doi.org/10.1016/j.orggeochem.2017.07.016

Douglas, P.M.J., Stolper, D.A., Smith, D.A., Walter Anthony, K.M., Paull, C.K., Dallimore, S., Wik, M., Crill, P.M., Winterdahl, M., Eiler, J.M., Sessions, A.L., 2016. Diverse origins of

Arctic and Subarctic methane point source emissions identified with multiply-substituted isotopologues. *Geochim. Cosmochim. Acta* **188**, 163–188. https://doi.org/10.1016/j.gca.2016.05.031

Dunning, T.H., 1989. Gaussian basis sets for use in correlated molecular calculations. I. The atoms boron through neon and hydrogen. *J. Chem. Phys*. **90**, 1007–1023. https://doi.org/10.1063/1.456153

Eggenkamp, H.G.M., 2004. Summary of Methods for Determining the Stable Isotope Composition of Chlorine and Bromine in Natural Materials, in: *Handbook of Stable Isotope Analytical Techniques*. Elsevier, pp. 604–622. https://doi.org/10.1016/B978-044451114-0/50030-2

Eiler, J.M., 2013. The Isotopic Anatomies of Molecules and Minerals. *Annu. Rev. Earth Planet. Sci.* **41**, 411–441. https://doi.org/10.1146/annurev-earth-042711-105348

Eiler, J.M., 2007. "Clumped-isotope" geochemistry—The study of naturally-occurring, multiply-substituted isotopologues. *Earth Planet. Sci. Lett*. **262**, 309–327. https://doi.org/10.1016/j.epsl.2007.08.020

Eiler, J.M., Clog, M., Magyar, P., Piasecki, A., Sessions, A., Stolper, D., Deerberg, M., Schlueter, H.-J., Schwieters, J., 2012. A high-resolution gas-source isotope ratio mass spectrometer. *Int. J. Mass Spectrom.*

Eiler, J.M., Schauble, E., 2004. $^{18}O^{13}C^{16}O$ in Earth's atmosphere. *Geochim. Cosmochim. Acta* **68**, 4767–4777.

Eldridge, D.L., Korol, R., Lloyd, M.K., Turner, A.C., Webb, M.A., Miller, T.F., Stolper, D.A., 2019. Comparison of Experimental vs Theoretical Abundances of $^{13}CH_3D$ and $^{12}CH_2D_2$ for Isotopically Equilibrated Systems from 1 to 500 °C. *ACS Earth Space Chem*. **3**, 2747–2764. https://doi.org/10.1021/acsearthspacechem.9b00244

Feakins, S.J., Ellsworth, P.V., Sternberg, L. da S.L., 2013. Lignin methoxyl hydrogen isotope ratios in a coastal ecosystem. *Geochim. Cosmochim. Acta* **121**, 54–66. https://doi.org/10.1016/j.gca.2013.07.012

M. J. Frisch, G. W. Trucks, H. B. Schlegel, G. E. Scuseria, M. A. Robb, J. R. Cheeseman, G. Scalmani, V. Barone, B. Mennucci, G. A. Petersson, H. Nakatsuji, M. Caricato, X. Li, H. P. Hratchian, A. F. Izmaylov, J. Bloino, G. Zheng, J. L. Sonnenberg, M. Hada, M. Ehara, K. Toyota, R. Fukuda, J. Hasegawa, M. Ishida, T. Nakajima, Y. Honda, O. Kitao, H. Nakai, T. Vreven, J. A. Montgomery, Jr.,. E. Peralta, F. Ogliaro, M. Bearpark, J. J. Heyd, E. Brothers, K. N. Kudin, V. N. Staroverov, T. Keith, R. Kobayashi, J. Normand, K. Raghavachari, A. Rendell, J. C. Burant, S. S. Iyengar, J. Tomasi, M. Cossi, N. Rega, J. M. Millam, M. Klene, J. E. Knox, J. B. Cross, V. Bakken, C. Adamo, J. Jaramillo, R. Gomperts, R. E. Stratmann, O. Yazyev, A. J. Austin, R. Cammi, C. Pomelli, J. W. Ochterski, R. L. Martin, K. Morokuma, V. G. Zakrzewski, G. A. Voth, P. Salvador, J. J. Dannenberg, S. Dapprich, A. D. Daniels, O. Farkas, J. B. Foresman, J. V. Ortiz, J. Cioslowski, and D. J. Fox, 2013. Gaussian 09, Revision E.01, Gaussian, Inc., Wallingford CT

Gehre, M., Renpenning, J., Geilmann, H., Qi, H., Coplen, T.B., Kümmel, S., Ivdra, N., Brand, W.A., Schimmelmann, A., 2017. Optimization of on-line hydrogen stable isotope ratio measurements of halogen- and sulfur-bearing organic compounds using elemental analyzer-chromium/high-temperature conversion isotope ratio mass spectrometry (EA-Cr/HTC-IRMS). *Rapid Comm. Mass. Spectrom*. **31**, 475-484.

Ghosh, P., Adkins, J., Affek, H., Balta, B., Guo, W., Schauble, E.A., Schrag, D., Eiler, J.M., 2006. $^{13}C–^{18}O$ bonds in carbonate minerals: A new kind of paleothermometer. *Geochimica et Cosmochimica Acta* **70**, 1439–1456. https://doi.org/10.1016/j.gca.2005.11.014

Giunta, T., Young, E.D., Warr, O., Kohl, I., Ash, J.L., Martini, A., Mundle, S.O.C., Rumble, D., Pérez-Rodríguez, I., Wasley, M., LaRowe, D.E., Gilbert, A., Sherwood Lollar, B., 2019. Methane sources and sinks in continental sedimentary systems: New insights from paired clumped isotopologues $^{13}CH_3D$ and $^{12}CH_2D_2$. *Geochim. Cosmochim. Acta* **245**, 327–351. https://doi.org/10.1016/j.gca.2018.10.030

Goldshleger, N.F., Tyabin, M.B., Shilov, A.E., Shteinman, A.A., 1969. Activation of Saturated Hydrocarbons. Deuterium-hydrogen exchange in solutions of transition metal complexes. *Russ. J. Phys. Chem*. **43**, 1222-+.

Greule, M., Moossen, H., Lloyd, M. K., Geilmann, H., Brand, W.A., Eiler, J.M., Qi, H., Keppler, F., 2019. Three wood isotopic reference materials for δ^2H and $\delta^{13}C$ measuremnts of plant methoxy groups. *Chemical Geology* **533**. 10.1016/j.chemgeo.2019.119428

Greule, M., Tumino, L.D., Kronewald, T., Hener, U., Schleucher, J., Mosandl, A., Keppler, F., 2010. Improved rapid authentication of vanillin using $\delta^{13}C$ and δ^2H values. *Eur. Food Res. Technol.* **231**, 933–941. https://doi.org/10.1007/s00217-010-1346-z

Gruen, D.S., Wang, D.T., Könneke, M., Topçuoğlu, B.D., Stewart, L.C., Goldhammer, T., Holden, J.F., Hinrichs, K.-U., Ono, S., 2018. Experimental investigation on the controls of clumped isotopologue and hydrogen isotope ratios in microbial methane. *Geochim. Cosmochim. Acta* **237**, 339–356. https://doi.org/10.1016/j.gca.2018.06.029

Guo, W., 2020. Kinetic clumped isotope fractionation in the DIC-H_2O-CO_2 system: Patterns, controls, and implications. *Geochim. Cosmochim. Acta* **268**, 230–257. https://doi.org/10.1016/j.gca.2019.07.055

Helms, C.R., Deal, B.E., 1992. Mechanisms of the HF/H 2 O vapor phase etching of SiO 2. *J. Vac. Sci. Technol. Vac. Surf. Films* **10**, 806–811. https://doi.org/10.1116/1.577676

Horibe, Y., Craig, H., 1995. DH fractionation in the system methane-hydrogen-water. *Geochim. Cosmochim. Acta* **59**, 5209–5217. https://doi.org/10.1016/0016-7037(95)00391-6

Huntington, K.W., Eiler, J.M., Affek, H.P., Guo, W., Bonifacie, M., Yeung, L.Y., Thiagarajan, N., Passey, B., Tripati, A., Daëron, M., Came, R., 2009. Methods and limitations of 'clumped' CO_2 isotope (Δ_{47}) analysis by gas-source isotope ratio mass spectrometry. *J. Mass Spectrom.* **44**, 1318–1329. https://doi.org/10.1002/jms.1614

Kendall, R.A., Dunning, T.H., Harrison, R.J., 1992. Electron affinities of the first-row atoms revisited. Systematic basis sets and wave functions. *J. Chem. Phys*. **96**, 6796-6806. 10.1063/1.462569

Keppler, F., Hamilton, J.T.G., McRoberts, W.C., Vigano, I., Braß, M., Röckmann, T., 2008. Methoxyl groups of plant pectin as a precursor of atmospheric methane: evidence from deuterium labelling studies. *New Phytol*. **178**, 808–814. https://doi.org/10.1111/j.1469-8137.2008.02411.x

Keppler, F., Harper, D.B., Kalin, R.M., Meier-Augenstein, W., Farmer, N., Davis, S., Schmidt, H.-L., Brown, D.M., Hamilton, J.T.G., 2007. Stable hydrogen isotope ratios of lignin methoxyl groups as a paleoclimate proxy and constraint of the geographical origin of wood. *New Phytol*. **176**, 600–609. https://doi.org/10.1111/j.1469-8137.2007.02213.x

Krueger, D.A., Krueger, H.W., 1983. Carbon isotopes in vanillin and the detection of falsified natural vanillin. *J. Agric. Food Chem*. **31**, 1265–1268. https://doi.org/10.1021/jf00120a030

Landgraf, B.J., McCarthy, E.L., Booker, S.J., 2016. Radical S-Adenosylmethionine Enzymes in Human Health and Disease. *Annu. Rev. Biochem*. **85**, 485–514. https://doi.org/10.1146/annurev-biochem-060713-035504

Lee, C., Yang, W., Parr, R.G., 1988. Development of the Colle-Salvetti correlation-energy formula into a functional of the electron density. *Phys. Rev. B* **37**, 785–789. 10.1103/PhysRevB.37.785

Lee, H., Feng, X., Mastalerz, M., Feakins, S.J., 2019. Characterizing lignin: Combining lignin phenol, methoxyl quantification, and dual stable carbon and hydrogen isotopic techniques. *Org. Geochem*. **136**, 103894. https://doi.org/10.1016/j.orggeochem.2019.07.003

Levin, N.E., Raub, T.D., Dauphas, N., Eiler, J.M., 2014. Triple oxygen isotope variations in sedimentary rocks. *Geochim. Cosmochim. Acta* **139**, 173–189. https://doi.org/10.1016/j.gca.2014.04.034

Lloyd, M.K., 2017. Clumped and intramolecular isotopic perspectives on the behavior of organic and inorganic carbon in the shallow crust and deep biosphere. PhD thesis, California Institute of Technology.

Loyd, S.J., Sample, J., Tripati, R.E., Defliese, W.F., Brooks, K., Hovland, M., Torres, M., Marlow, J., Hancock, L.G., Martin, R., Lyons, T., Tripati, A.E., 2016. Methane seep carbonates yield clumped isotopesignatures out of equilibrium with formation temperatures. *Nat. Commun.* **7**, 1–12. https://doi.org/10.1038/ncomms12274

Maccoll, A., 1969. Heterolysis and the Pyrolysis of Alkyl Halides in the Gas Phase. *Chem. Rev.* 69, 33–60. https://doi.org/10.1021/cr60257a002

Magyar, P.M., 2017. Insights into pathways of nitrous oxide generation from novel isotopologue measurements. PhD thesis, California Institute of Technology.

Magyar, P.M., Orphan, V.J., Eiler, J.M., 2016. Measurement of rare isotopologues of nitrous oxide by high-resolution multi-collector. *Rapid Commun. Mass Spectrom*. **30**, 1923–1940. https://doi.org/10.1002/rcm.7671

Mann, J., 1987. Modern methods for the introduction of fluorine into organic molecules: an approach to compounds with altered chemical and biological activities. *Chem. Soc. Rev*. **16**, 381–436. https://doi.org/10.1039/CS9871600381

Møller, Chr., Plesset, M.S., 1934. Note on an Approximation Treatment for Many-Electron Systems. *Phys. Rev*. **46**, 618–622. https://doi.org/10.1103/PhysRev.46.618

Morrison, J.A., Nakayama, K., 1963. Reaction of single crystals of potassium bromide with chlorine gas. *Trans. Faraday Soc*. **59**, 2560. https://doi.org/10.1039/tf9635902560

Ohligschläger, A., Menzel, K., Kate, A.T., Martinez, J.R., Frömbgen, C., Arts, J., McCulloch, A., Rossberg, M., Lendle, W., Pfleiderer, G., Tögel, A., Torkelson, T.R., Beutel, K.K., 2019. Chloromethanes, in: *Ullmann's Encyclopedia of Industrial Chemistry*, pp. 1–31. https://doi.org/10.1002/14356007.a06_233.pub4

Olah, G.A., Gupta, B., Felberg, J.D., Ip, W.M., Husain, A., Karpeles, R., Lammertsma, K., Melhotra, A.K., Trivedi, N.J., 1985. Electrophilic reactions at single bonds. 20. Selective monohalogenation of methane over supported acidic or platinum metal catalysts and hydrolysis of methyl halides over .gamma.-alumina-supported metal oxide/hydroxide catalysts. A feasible path for the oxidative conversion of methane into methyl

alcohol/dimethyl ether. *J. Am. Chem. Soc*. **107**, 7097–7105. https://doi.org/10.1021/ja00310a057

Ono, S., Wang, D.T., Gruen, D.S., Sherwood Lollar, B., Zahniser, M.S., McManus, B.J., Nelson, D.D., 2014. Measurement of a doubly substituted methane isotopologue, $^{13}CH_3D$, by tunable infrared laser direct absorption spectroscopy. *Anal. Chem*. **86**, 6487-6494. https://doi.org/10.1021/ac5010579

Ono, S., Wing, B., Johnston, D., Farquhar, J., Rumble, D., 2006. Mass-dependent fractionation of quadruple stable sulfur isotope system as a new tracer of sulfur biogeochemical cycles. *Geochim. Cosmochim. Acta* **70**, 2238–2252. https://doi.org/10.1016/j.gca.2006.01.022

Ott, J., Gronemann, V., Pontzen, F., Fiedler, E., Grossmann, G., Kersebohm, D.B., Weiss, G., Witte, C., 2012. Methanol, in: *Ullmann's Encyclopedia of Industrial Chemistry*. American Cancer Society. https://doi.org/10.1002/14356007.a16_465.pub3

Popa, M.E., Paul, D., Janssen, C., Röckmann, T., 2018. H_2 clumped isotope measurements at natural isotopic abundances. *Rapid Comm. Mass. Spectrom*. **33**, 239-251.

Purvis, G.D., Bartlett, R.J., 1982. A full coupled-cluster singles and doubles model: The inclusion of disconnected triples. *J. Chem. Phys*. **76**, 1910–1918. https://doi.org/10.1063/1.443164

Rahikainen, M., Alegre, S., Trotta, A., Pascual, J., Kangasjärvi, S., 2018. Trans-methylation reactions in plants: focus on the activated methyl cycle. *Physiol. Plant*. **162**, 162–176. https://doi.org/10.1111/ppl.12619

Robertson, K.D., 2005. DNA methylation and human disease. *Nat. Rev. Genet*. **6**, 597–610. https://doi.org/10.1038/nrg1655

Roje, S., 2006. S-Adenosyl-l-methionine: Beyond the universal methyl group donor. Rod Croteau Spec. Issue Part 1 **67**, 1686–1698. https://doi.org/10.1016/j.phytochem.2006.04.019

San Filippo, J., Romano, L.J., 1975. Mechanism of the reaction of alkyl bromides and iodides with mercury(II) and silver(I) fluorides. *J. Org. Chem*. **40**, 782–787. https://doi.org/10.1021/jo00894a022

Schimmelmann, A., Qi, H., Coplen, T.B., Brand, W.A., Fong, J., Meier-Augenstein, W., Kemp, H.F., Toman, B., Ackermann, A., Assonov, S., Aerts-Bijma, A.T., Brejcha, R., Chikaraishi, Y., Darwish, T., Elsner, M., Gehre, M., Geilmann, H., Gröning, M., Hélie, J.-F., Herrero-Martín, S., Meijer, H.A.J., Sauer, P.E., Sessions, A.L., Werner, R.A., 2016. Organic Reference Materials for Hydrogen, Carbon, and Nitrogen Stable Isotope-Ratio Measurements: Caffeines, n-Alkanes, Fatty Acid Methyl Esters, Glycines, l-Valines, Polyethylenes, and Oils. *Anal. Chem*. **88**, 4294–4302. https://doi.org/10.1021/acs.analchem.5b04392

Schmidt, H.-L, Robins, R.J., Werner, R.A., 2015. Multi-factorial *in vivo* stable isotope fractionation: causes, correlations, consequences and applications. *Isotopes in Environ. and Heal. Stud.* **51**. 155–199. https://doi.org/10.1080/10256016.2015.1014355

Selin, N., 2009. Global biogeochemical cycling of mercury: A review. *Annu. Rev. Environ. Resour.* **34**, 43–63.

Siegemund, G., Schwertfeger, W., Feiring, A., Smart, B., Behr, F., Vogel, H., McKusick, B., Kirsch, P., 2016. Fluorine Compounds, Organic, in: *Ullmann's Encyclopedia of Industrial Chemistry*. American Cancer Society, pp. 1–56. https://doi.org/10.1002/14356007.a11_349.pub2

Stolper, D.A., Sessions, A.L., Ferreira, A.A., Neto, E.V.S., Schimmelmann, A., Shusta, S.S., Valentine, D.L., Eiler, J.M., 2014a. Combined ^{13}C–D and D–D clumping in methane: Methods and preliminary results. *Geochimica et Cosmochimica Acta* **126**, 169–191. https://doi.org/10.1016/j.gca.2013.10.045

Stolper, D.A., Lawson, M., Davis, C.L., Ferreira, A.A., Neto, E.V.S., Ellis, G.S., Lewan, M.D., Martini, A.M., Tang, Y., Schoell, M., Sessions, A.L., Eiler, J.M., 2014b. Formation temperatures of thermogenic and biogenic methane. *Science* **344**, 1500–1503. https://doi.org/10.1126/science.1254509

Stolper, D.A., Martini, A.M., Clog, M., Douglas, P.M., Shusta, S.S., Valentine, D.L., Sessions, A.L., Eiler, J.M., **2015**. Distinguishing and understanding thermogenic and biogenic sources of methane using multiply substituted isotopologues. *Geochim. Cosmochim. Acta* 161, 219–247.

Taenzer, L., Labidi, J., Masterson, A.L., Feng, X., Rumble, D., Young, E.D., Leavitt, W.D., **2020**. Low $\Delta^{12}CH_2D_2$ values in microbialgenic methane result from combinatorial isotope effects. *Geochim. Cosmochim. Acta* 285, 225–236. 10.1016/j.gca.2020.06.026

Tenailleau, E.J., Lancelin, P., Robins, R.J. and, Akoka, S., 2004. Authentication of the Origin of Vanillin Using Quantitative Natural Abundance ^{13}C NMR. *J. Agric. Food Chem*. **52**, 7782–7787. https://doi.org/10.1021/jf048847s

Tripati, A.K., Hill, P.S., Eagle, R.A., Mosenfelder, J.L., Tang, J., Schauble, E.A., Eiler, J.M., Zeebe, R.E., Uchikawa, J., Coplen, T.B., Ries, J.B., Henry, D., 2015. Beyond temperature: Clumped isotope signatures in dissolved inorganic carbon species and the influence of solution chemistry on carbonate mineral composition. *Geochim. Cosmochim. Acta* https://doi.org/10.1016/j.gca.2015.06.021

Urey, H.C., 1947. The thermodynamic properties of isotopic substances. *J. Chem. Soc.* Resumed 562–581.

Wang, D.T., Gruen, D.S., Lollar, B.S., Hinrichs, K.-U., Stewart, L.C., Holden, J.F., Hristov, A.N., Pohlman, J.W., Morrill, P.L., Könneke, M., Delwiche, K.B., Reeves, E.P., Sutcliffe, C.N., Ritter, D.J., Seewald, J.S., McIntosh, J.C., Hemond, H.F., Kubo, M.D., Cardace, D., Hoehler, T.M., Ono, S., 2015. Nonequilibrium clumped isotope signals in microbial methane. *Science* **348**, 428. https://doi.org/10.1126/science.aaa4326

Wang, D.T., Welander, P.V., Ono, S., 2016. Fractionation of the methane isotopologues 13CH4, $^{12}CH_3D$, and $^{13}CH_3D$ during aerobic oxidation of methane by Methylococcus capsulatus (Bath). *Geochim. Cosmochim. Acta* **192**, 186–202. https://doi.org/10.1016/j.gca.2016.07.031

Wang, Z., Schauble, E.A., Eiler, J.M., 2004. Equilibrium thermodynamics of multiply substituted isotopologues of molecular gases. *Geochim. Cosmochim. Acta* **68**, 4779–4797. https://doi.org/10.1016/j.gca.2004.05.039

Watkins, J.M., Hunt, J.D., 2015. A process-based model for non-equilibrium clumped isotope effects in carbonates. *Earth Planet. Sci. Lett*. **432**, 152–165. https://doi.org/10.1016/j.epsl.2015.09.042

Webb, M.A., Miller, T.F., 2013. Position-specific and Clumped Stable Isotope Studies: Comparison of the Urey and Path-Integral Approaches for Carbon Dioxide, Nitrous Oxide, Methane, and Propane. *J. Phys. Chem. A* 131227163831000. https://doi.org/10.1021/jp411134v

Weissman, M., Benson, S.W., 1984. Pyrolysis of methyl chloride, a pathway in the chlorine-catalyzed polymerization of methane. *Int. J. Chem. Kinet*. **16**, 307–333. https://doi.org/10.1002/kin.550160403

Wilkinson, J.A., 1992. Recent advances in the selective formation of the carbon-fluorine bond. *Chem. Rev*. **92**, 505–519. https://doi.org/10.1021/cr00012a002

Wu, Y.-P., Won, Y.-S., 2000. Pyrolysis of chloromethanes. *Combust. Flame* **122**, 312–326. https://doi.org/10.1016/S0010-2180(00)00116-4

Xie, H., Ponton, C., Formolo, M.J., Lawson, M., Peterson, B.K., Lloyd, M.K., Sessions, A.L., Eiler, J.M., 2018. Position-specific hydrogen isotope equilibrium in propane. *Geochim. Cosmochim. Acta* **238**, 193–207. https://doi.org/10.1016/j.gca.2018.06.025

Xie, H., Dong, G., Thiagaranjan, N., Shuai, Y., Mangenot, X., Formolo, M.J., Eiler, J.M., 2019. Methane clumped isotopologues with high-resolution gas source isotope ratio mass spectrometry. AGU Fall Meeting, December 2019. http://adsabs.harvard.edu/abs/2019AGUFM.V14B..05X.

Yeung, L.Y., 2016. Combinatorial effects on clumped isotopes and their significance in biogeochemistry. *Geochim. Cosmochim. Acta* **172**, 22–38.

Yeung, L.Y., Ash, J.L., Young, E.D., 2015. Biological signatures in clumped isotopes of O_2. *Science* **348**, 431–434. https://doi.org/10.1126/science.aaa6284

Yeung, L.Y., Haslun, J.A., Ostrom, N.E., Sun, T., Young, E.D., van Kessel, M.A.H.J., Lücker, S., Jetten, M.S.M., 2019. In Situ Quantification of Biological N_2 Production Using Naturally Occurring $^{15}N^{15}N$. *Environ. Sci. Technol*. **53**, 5168–5175. https://doi.org/10.1021/acs.est.9b00812

Yeung, L.Y., Li, S., Kohl, I.E., Haslun, J.A., Ostrom, N.E., Hu, H., Fischer, T.P., Schauble, E.A., Young, E.D., 2017. Extreme enrichment in atmospheric $^{15}N^{15}N$. *Sci. Adv*. **3**, eaao6741. https://doi.org/10.1126/sciadv.aao6741

Yeung, L.Y., Murray, L.T., Ash, J.L., Young, E.D., 2016. Isotopic ordering in atmospheric O_2 as a tracer of ozone photochemistry and the tropical atmosphere. *J. Geophys. Res. Atmos*., **121**. https://doi.org/10.1002/(ISSN)2169-8996

Yeung, L.Y., Young, E.D., Schuable, E.A., 2012. Measurements of $^{18}O^{18}O$ and $^{17}O^{18}O$ in the atmosphere and the role of isotope-exchange reactions. *J. Geophys. Res. Atmos*. **117**. https://doi.org/10.1029/2012JD017992

Young, E.D., Kohl, I.E., Lollar, B.S., Etiope, G., Rumble III, D., Li 李姝宁, S., Haghnegahdar, M.A., Schauble, E.A., McCain, K.A., Foustoukos, D.I., Sutclife, C., Warr, O., Ballentine, C.J., Onstott, T.C., Hosgormez, H., Neubeck, A., Marques, J.M., Pérez-Rodríguez, I., Rowe, A.R., LaRowe, D.E., Magnabosco, C., Yeung, L.Y., Ash, J.L., Bryndzia, L.T., 2017. The relative abundances of resolved $^{12}CH_2D_2$ and $^{13}CH_3D$ and mechanisms controlling isotopic bond ordering in abiotic and biotic methane gases. *Geochim. Cosmochim. Acta* **203**, 235–264.

Young, E.D., Rumble, D., Freedman, P., Mills, M., 2016. A large-radius high-mass-resolution multiple-collector isotope ratio mass spectrometer for analysis of rare isotopologues of O2, N2, CH4, and other gases. *Int. Jour. Mass. Spec.* **401**, 1-10.

Zeisel, S., 1885. Über ein Verfahren zum quantitativen Nachweise von Methoxyl. *Monatshefte Für Chem*. **6**, 989–997. https://doi.org/10.1007/BF01554683

1569

Figures and Figure Captions

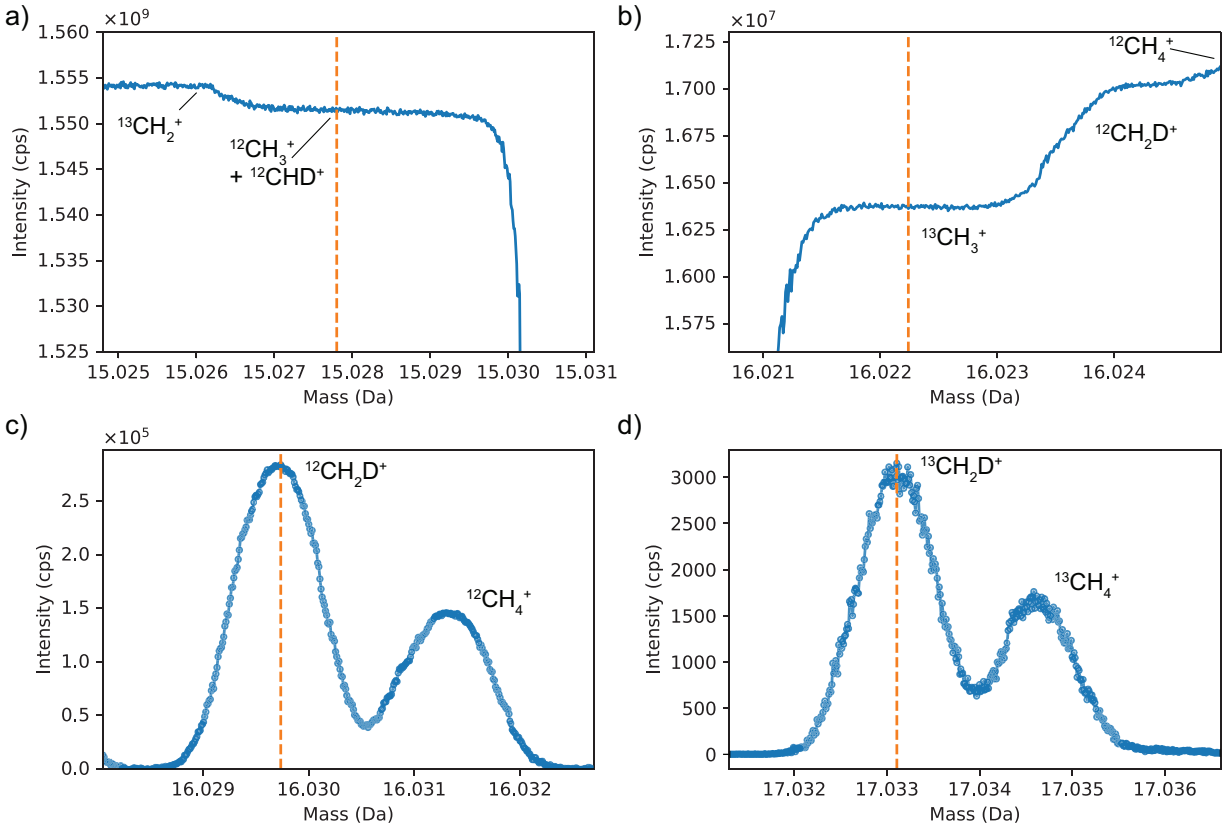

Figure 1: Mass scans of isotopologues of methyl fragments of CH_3F used to determine δD (a + c), δ^{13}C (a + b), and $\delta^{13}CH_2D$ (a + d). Scans were made under typical measurement conditions. Orange dashed lines indicate measurement locations. Mass 15 Da scan in a) has been corrected for signal decay due to pressure bleed-out. $^{12}CHD^+$ is not resolved and is corrected for in post-measurement processing (see Appendix A1). b) Resolution of $^{13}CH_3^+$ from $^{12}CH_2D^+$. Typical mass resolving power (MRP, 5–95% definition) is 16,000. $^{13}CH_3^+$ integrations are corrected for possible background $^{14}NH_2^+$ contamination by integrating the background at the location shown in Fig. 2b. c) Measurement of $^{12}CH_2D^+$ resolved from $^{12}CH_4^+$. Typical MRP is 22,000. d) Measurement of $^{13}CH_2D^+$ resolved from $^{13}CH_4^+$. Typical MRP is 22,000.

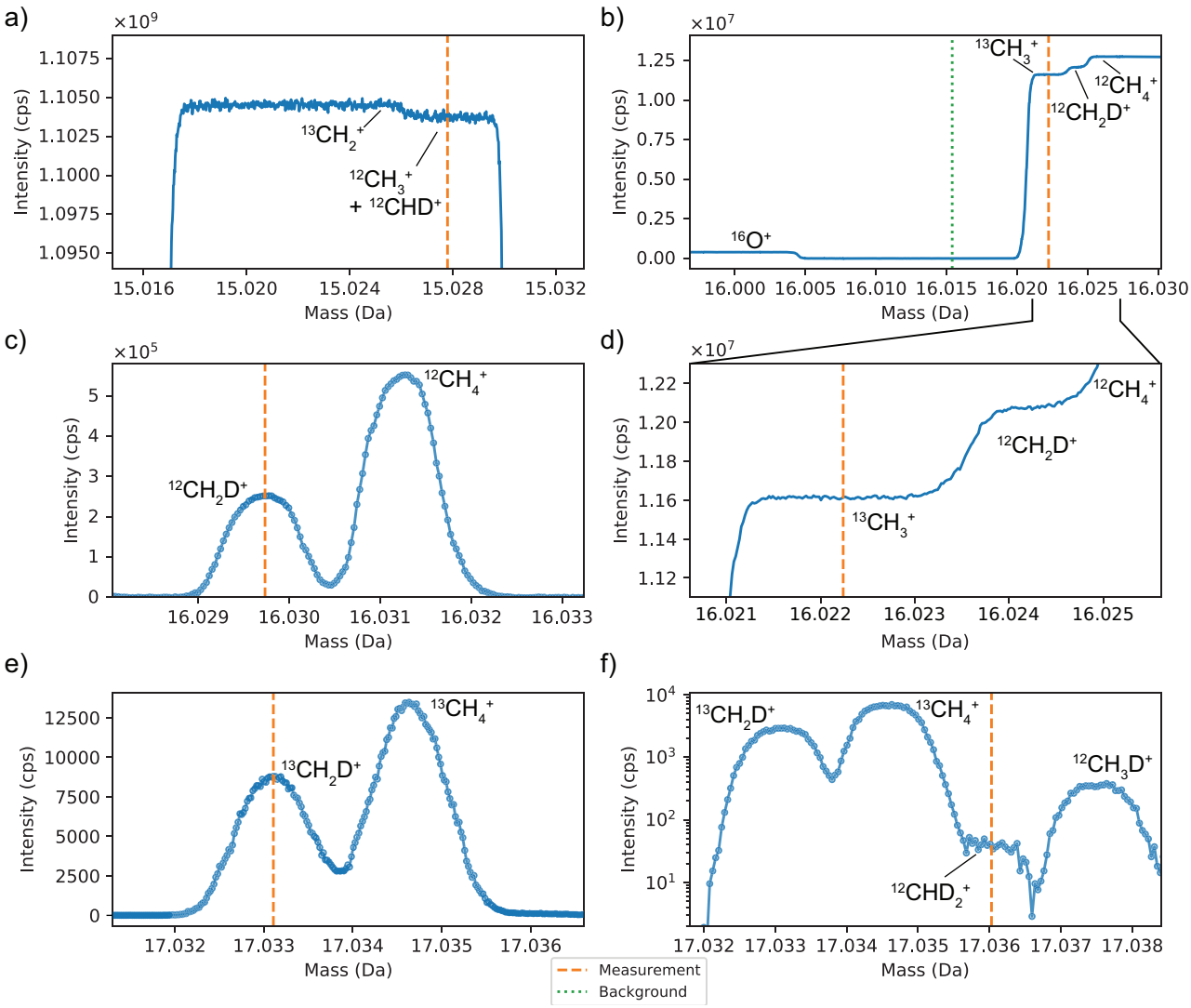

Figure 2: Mass spectrum scans of CH_3Cl methyl fragments used for δD (a + c), $\delta^{13}C$ (a + b), $\delta^{13}CH_2D$ (e + a), and $\delta^{12}CHD_2$ (f + a) determinations. Scans were made under typical measurement conditions. Orange dashed lines indicate mass spectrum locations where integrations are made. a) Mass 15 flat shoulder where $^{12}CH_3^+$ is resolved from $^{13}CH_2^+$. $^{12}CHD^+$ is not resolved and is corrected for in post-measurement processing. The scan has been corrected for signal loss due to pressure bleed-out. Mass resolving power (MRP; 5-95% definition) varies depending on measurement; see Table A2 for details). b) Resolution of $^{13}CH_3^+$ from $^{16}O^+$ and $^{12}CH_2D^+$. Green dashed line indicates location of background integrations for each $\delta^{13}C$ measurement. Typical MRP for $\delta^{13}C$ measurement is 16,000. c) Measurement of $^{12}CH_2D^+$ on the H4 cup with separation from the $^{12}CH_4^+$ H-adduct. $^{13}CH_3$ is at a lower mass and fully resolved. Typical MRP for δD measurement on H4 cup is 28,000. d) Zoomed-in view of singly substituted methyl fragments from showing flat $^{13}CH_3^+$ shoulder. e) Measurement of $^{13}CH_2D^+$ where resolved from $^{13}CH_4^+$. Typical MRP is 22,000. f) Measurement of $^{12}CHD_2^+$ is largely resolved from the $^{13}CH_4^+$ and $^{13}CH_3D^+$ adducts, but a tailing correction is applied. Procedures for this tailing correction are detailed in the Appendix Fig. A8. Typical MRP is 28,000.

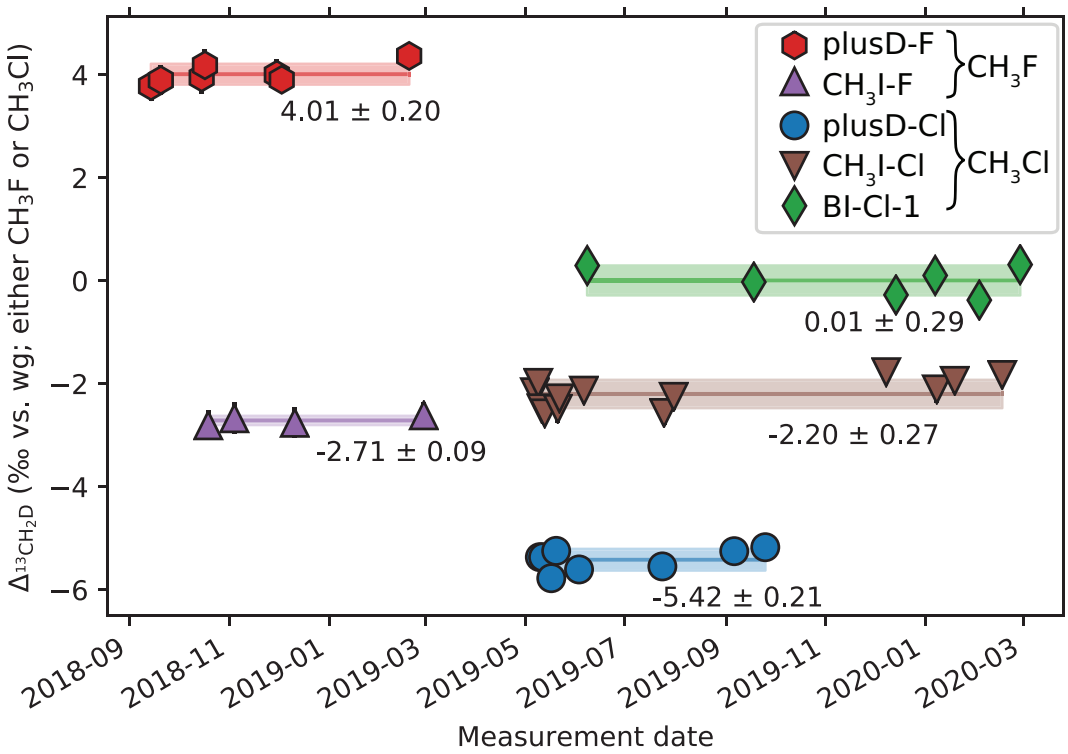

Figure 3: Reproducibility of $\Delta_{^{13}CH_2D}$ measurements of CH_3F and CH_3Cl standards vs. measurement date. $\Delta_{^{13}CH_2D}$ values are reported in ‰ relative to the corresponding working reference gas, either BIL-F-1 (for CH_3F measurements) or CIT-Cl-2 (for CH_3Cl measurements). Error bars on data points are ±1 s.e. (internal measurement errors). Mean values and $\pm 1\sigma$ for each standard are shown in solid lines and shaded boxes. Multi-week time gaps between measurements indicate intervals where methane was analyzed on the same instrument, or maintenance periods.

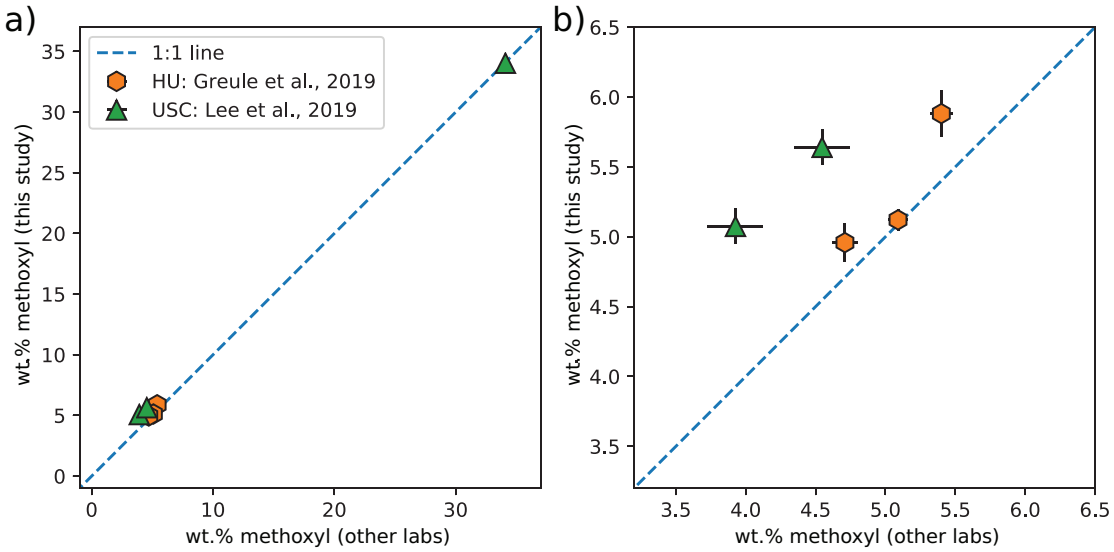

Figure 4: a): Measured abundance of methoxyl groups (in weight percent O-CH_3) vs. external values. External value of the syringaldehyde standard is the theoretical abundance based on its molecular formula (Lee et al., 2019). b) Zoomed-in view of a) on the methoxyl contents of woods. Error bars are $\pm 1\sigma$ of replicates; for samples that were measured once, error bars are the mean 1σ of all samples that were replicated (specifically, 0.09 %). Error bars on external values are from the original publications.

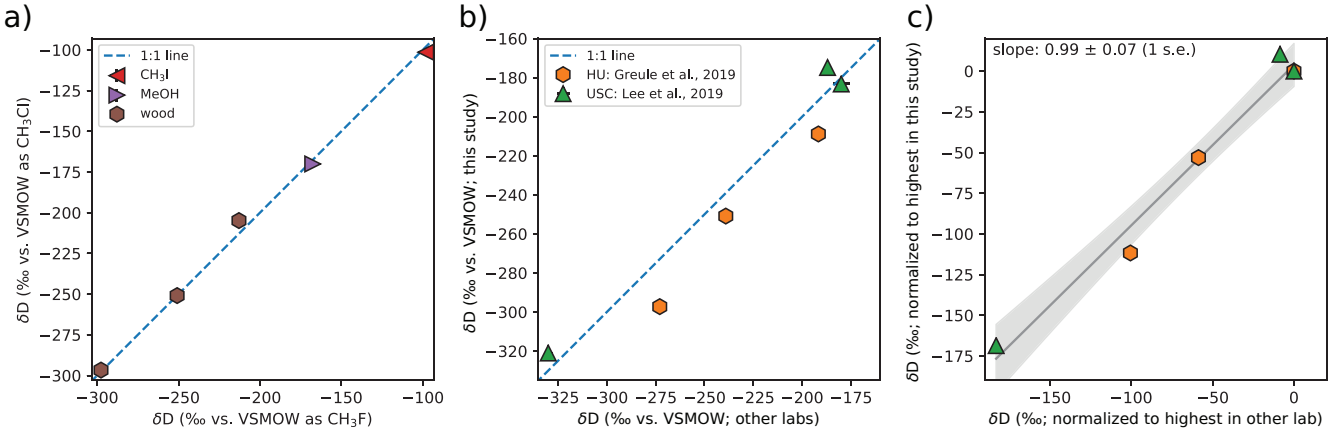

Figure 5: Tests of δD accuracy. a) Comparison of δD values of materials measured here as CH_3Cl and CH_3F. Each point is the average of all replicates measured as the same analyte gas. We provide a 1:1 line is given for comparison. B) δD values from this study vs. external values of wood and syringaldehyde standards measured by other laboratories. The 1:1 line is given for comparison. c) Relative differences in δD values normalized to the highest value reported in each laboratory. Grey line is a linear regression to the normalized data in this space. Grey envelope is the 95% confidence interval. In all panels, error bars on our measurements are ±1 s.e. of replicates; for samples that were measured only once, error bars are the mean 1σ of all samples that were replicated (specifically, 2.03 ‰). Error bars on external values are from the original publications. When not shown, error bars are smaller than symbols.

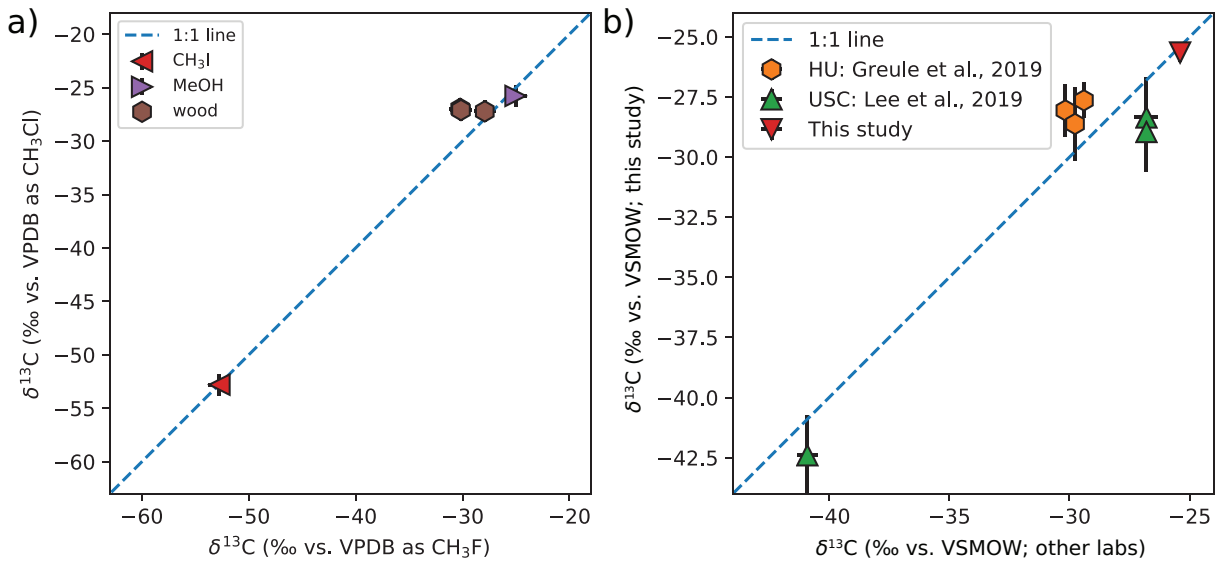

Figure 6: Tests of $\delta^{13}C$ accuracy. a) Comparison of internal $\delta^{13}C$ values of samples measured as CH_3Cl and CH_3F. Each point is the average of all replicates measured as the same analyte gas. 1:1 line also shown for comparison. b) $\delta^{13}C$ values from this study (internal) vs. external values of wood and syringaldehyde standards or the methanol standard measured in this study by conventional methods. A 1:1 line shown for comparison. In both panels, error bars on our measurements are ±1 s.e. of replicates; for samples that were measured once, error bars are the mean 1σ of all samples that were replicated (specifically, 1.59 ‰). Error bars on external values are from the original publications.

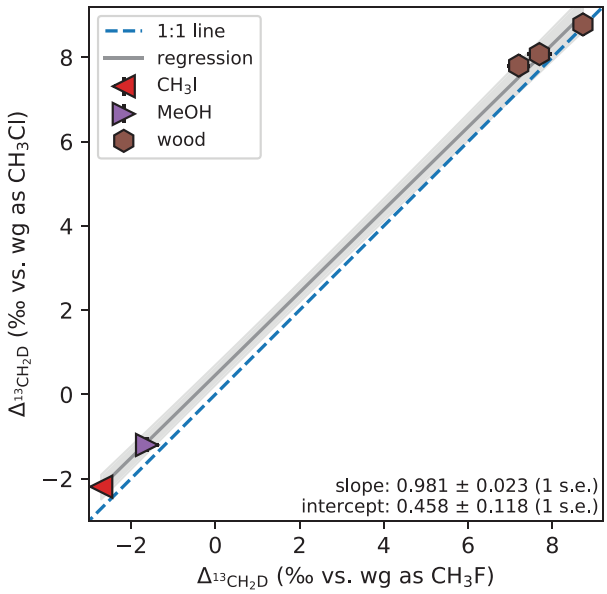

Figure 7: Comparison of $\Delta_{^{13}CH_2D}$ values of materials measured as CH_3Cl vs. as CH_3F. Error bars on points are ±1 s.e. of the mean. Error-weighted York regression ± 95% confidence interval are shown in grey (York, 1968). Blue dashed line is the 1:1 line. The slope of the regression is indistinguishable from 1 (see bottom right corner) indicating relative accuracy of measurements regardless of analyte. The intercept of the regression indicates the offset between the $\Delta_{^{13}CH_2D}$ values of the CH_3F and CH_3Cl working reference tanks in the thermodynamic reference frame.

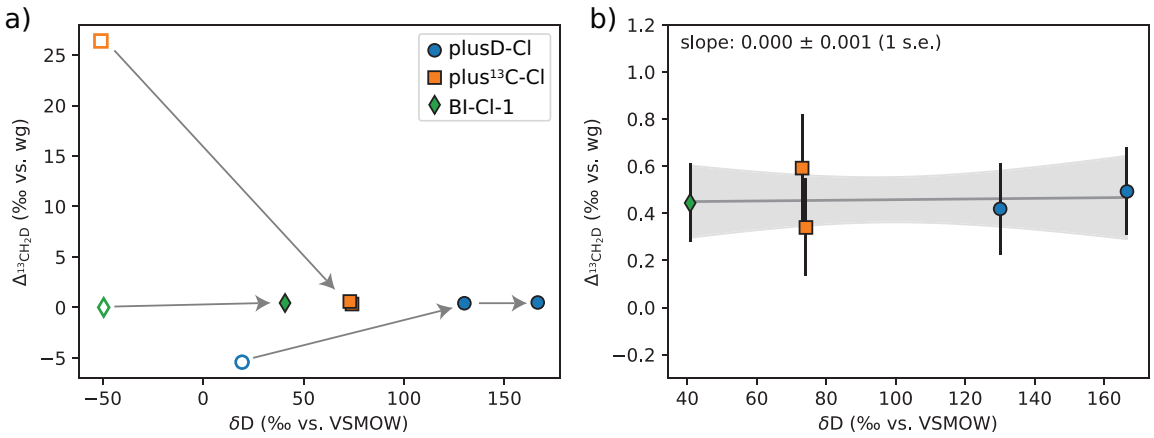

Figure 8: $\Delta_{^{13}CH_2D}$ values from CH_3Cl isotope-exchange experiments catalyzed on Pt/Al_2O_3 at 200 °C. Outlined symbols indicate mean values of starting gas compositions. Filled symbols indicate samples exposed to the catalyst at 200 °C for 90–185 hours. Arrows indicate direction of increased reaction time, but note that all points are separate experiments. b) is zoom-in of a) on samples we interpret to have equilibrated. Error bars in a) are smaller than the symbol size. Error bars in b) are ±1 s.e. Also shown in b) is the linear regression of $\Delta_{^{13}CH_2D}$ vs. δD among the equilibrated samples. Gray shading is the 95% confidence interval of the regression. The slope of the regression is within error of 0, indicating a lack of dependence of equilibrated $\Delta_{^{13}CH_2D}$ values on bulk isotopic composition.

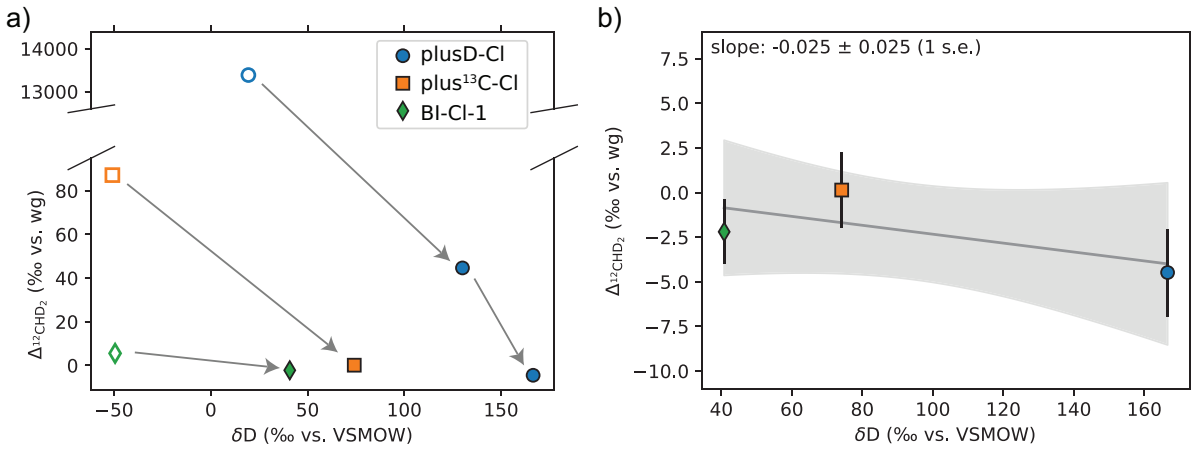

Figure 9: $\Delta_{12}{}_{CHD_2}$ values from CH_3Cl exchange experiments on Pt/Al_2O_3 at 200 °C. Symbols, arrows, and error bars are as in Figure 8. Arrows indicate direction of increased reaction time, but note that all points are separate experiments. Note broken axis indicating that the starting $\Delta_{12}{}_{CHD_2}$ value of the plusD-Cl standard is ~13,390 ‰. b) is a zoom in of a) on samples we interpret to have equilibrated. The slope of the regression is within error of 0, indicating a lack of dependence of $\Delta_{12}{}_{CHD_2}$ on bulk isotopic composition at equilibrium.

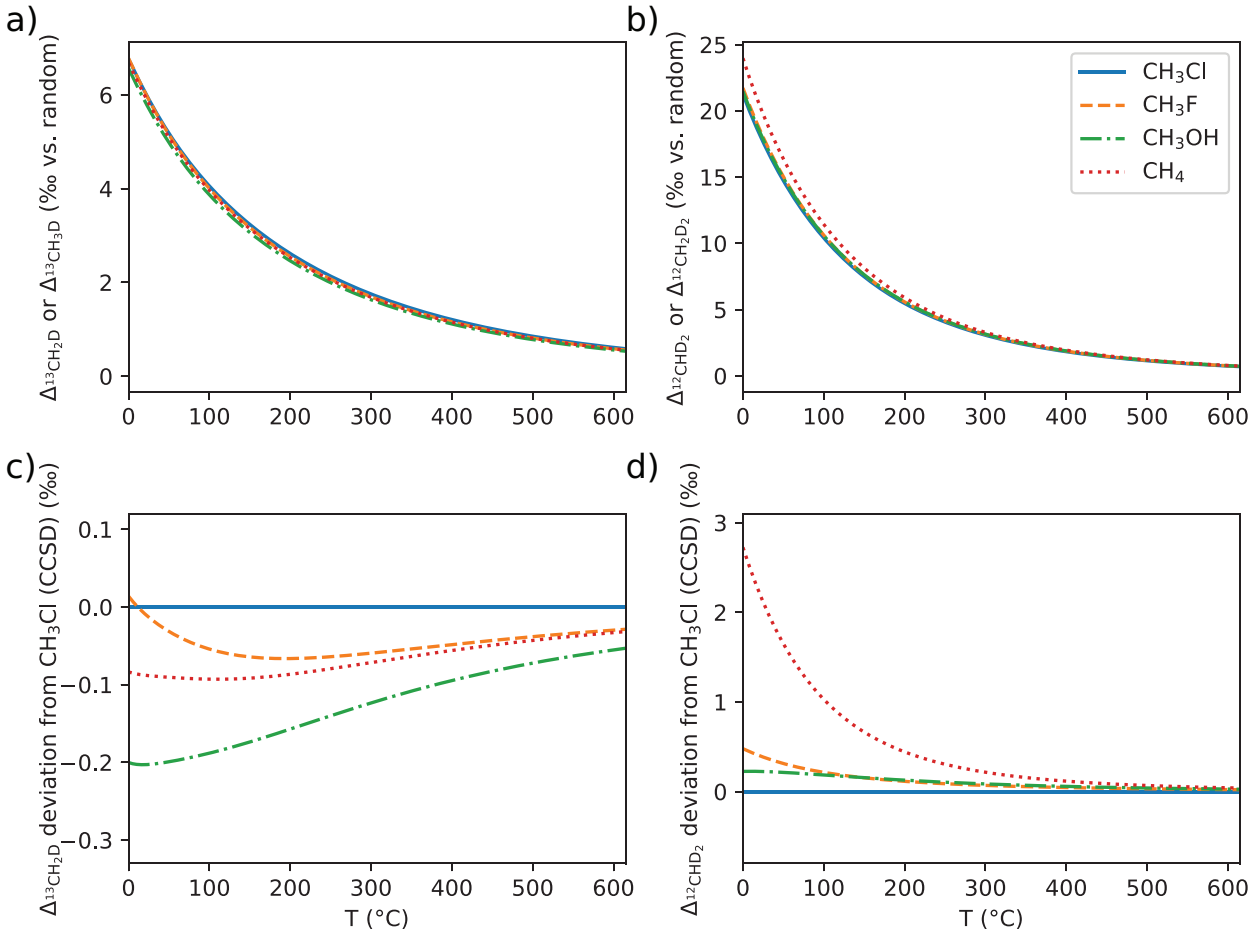

Figure 10: Theoretical predictions for the equilibrium dependencies of $\Delta_{^{13}CH_2D}$ and $\Delta_{^{12}CHD_2}$ values on temperature for simple methyl-containing molecules and for $\Delta_{^{13}CH_3D}$ and $\Delta_{^{12}CH_2D_2}$ in methane. All calculations performed with the aug-cc-pVTZ basis set at the CCSD level of theory (the highest levels explored for basis set size and theoretical level). a) $\Delta_{^{13}CH_2D}$ (and $\Delta_{^{13}CH_3D}$) predictions for the temperature range of 0–600 °C. b) $\Delta_{^{12}CHD_2}$ (and $\Delta_{^{12}CH_2D_2}$) predictions for the temperature range of 0–600 °C. c) $\Delta_{^{13}CH_2D}$ difference for each molecule from the $\Delta_{^{13}CH_2D}$ prediction for CH_3Cl. d) $\Delta_{^{12}CHD_2}$ difference for each molecule from the $\Delta_{^{12}CHD_2}$ prediction for CH_3Cl. Comparisons to other basis sets and levels of theory are shown in Appendix Figs. A6 and A7.

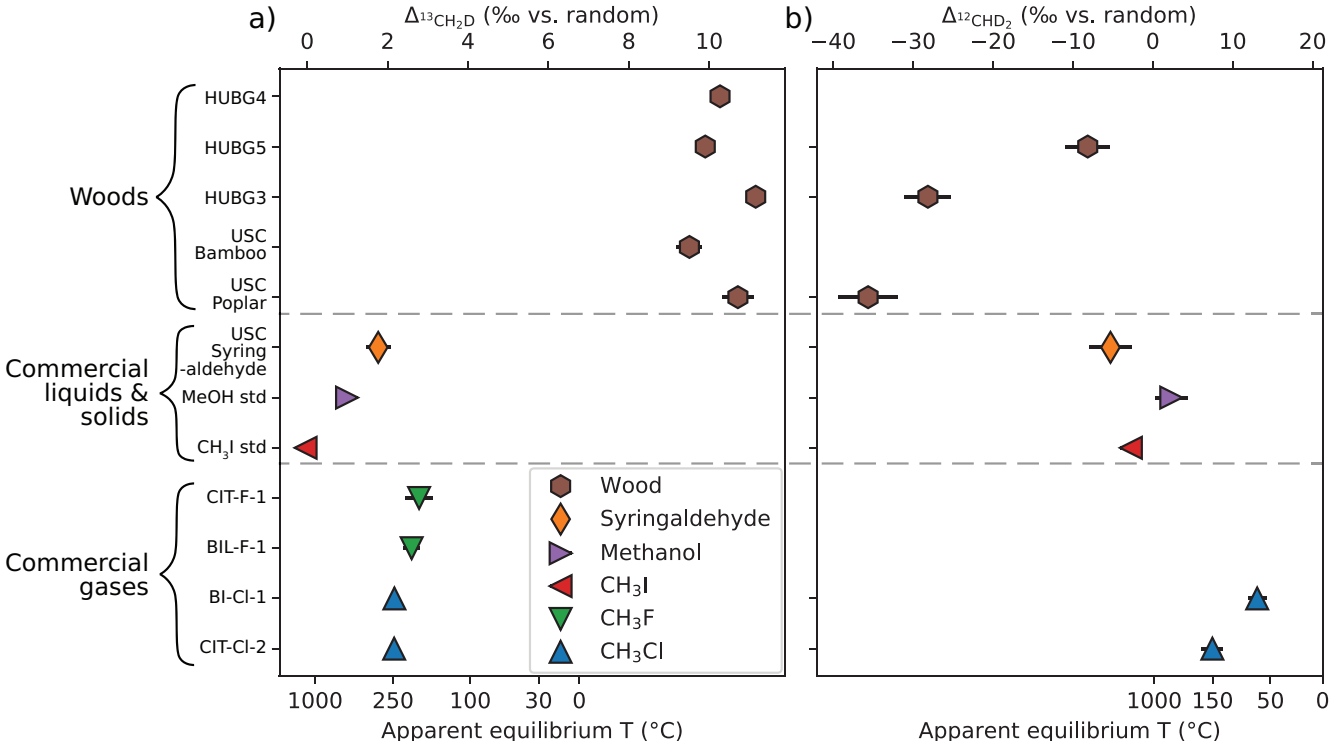

Figure 11: The clumped-isotope compositions commercial methyl and wood methoxyl groups. a): $\Delta_{13}{}_{CH_2D}$ values, b): $\Delta_{12}{}_{CHD_2}$ values. Samples are organized by material type. Bottom axis denotes apparent equilibrium temperatures in the thermodynamic CH_3Cl reference frame (Eqns. 17, 18). Error bars are ±1 s.e., see Table 5 for details.

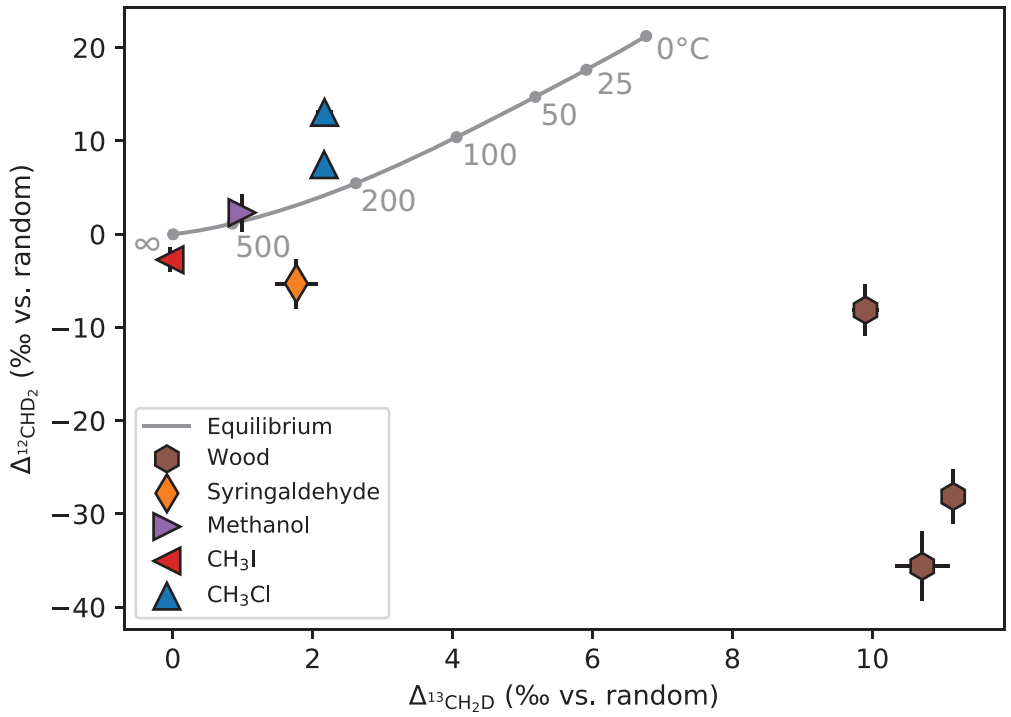

Figure 12: $\Delta_{12}CHD_2$ values vs. $\Delta_{13}CH_2D$ values of commercial compounds and woods. Grey curve is the line segment denoting mutual equilibrium: the theoretical relationship for CH_3Cl from 0 °C to ∞ (computed at the CCSD level of theory, aug-cc-pVTZ basis set; see Fig. 10, Eqns. 17, 18), where the equilibrium temperatures corresponding to $\Delta_{13}CH_2D$ and $\Delta_{12}CHD_2$ values are in agreement. Error bars are ±1 s.e., see Table 5 for details.